Federal University of Espírito Santo
Technology Center
Postgraduate Program in Electrical Engineering
Master Thesis

Pablo Rafael Neves Marciano

Design and Evaluation of a Low Complexity All-Optical OFDM System Applied to Passive Optical Networks

Vitória, ES, Brazil
April 2019

Pablo Rafael Neves Marciano

Design and Evaluation of a Low Complexity All-Optical OFDM System Applied to Passive Optical Networks

This Master thesis was submitted to the Postgraduate Program in Electrical Engineering from the Technology Center of the Federal University of Espírito Santo, as partial requirement for the degree of Master in Electrical Engineering.

Federal University of Espírito Santo – UFES

Electrical Engineering Department

Postgraduation Program

Supervisor: Marcelo Eduardo Vieira Segatto

Co-supervisor: Maria José Pontes

Vitória, ES, Brazil

April 2019

Pablo Rafael Neves Marciano

Design and Evaluation of a Low Complexity All-Optical OFDM System Applied to Passive Optical Networks/ Pablo Rafael Neves Marciano. – Vitória, ES, Brazil, April 2019-

87 p. : il. (some colors.) ; 30 cm.

Supervisor: Marcelo Eduardo Vieira Segatto

Co-supervisor: Maria José Pontes

Thesis (Masters) – Federal University of Espírito Santo – UFES
Electrical Engineering Department
Postgraduation Program, April 2019.

1. All-optical OFDM. 2. OFCS. 2. RFS. I. Marcelo E. V. Segatto. II. Maria J. Pontes. III. Federal University of Espírito Santo (UFES). IV. Electrical Engineering graduate program. V. Dissertation Title

Pablo Rafael Neves Marciano

Design and Evaluation of a Low Complexity All-Optical OFDM System Applied to Passive Optical Networks

This Master thesis was submitted to the Postgraduate Program in Electrical Engineering from the Technology Center of the Federal University of Espírito Santo, as partial requirement for the degree of Master in Electrical Engineering.

Work approved. Vitória, ES, Brazil, 12th of April, 2019:

Marcelo Eduardo Vieira Segatto
Supervisor

Maria José Pontes
Co-Supervisor

Prof. PhD. Maria Thereza Miranda Rocco Giraldi
Militar Institute of Engineering

Prof. PhD. Ciaran Patrick Moore
University of Canterbury, New Zealand

Vitória, ES, Brazil

April 2019

This work is dedicated to all who seeks the unrevealed truth.

Acknowledgements

First I want to thank God for giving me the strength to proceed and conclude my research. Secondly, I want to thank my family for supporting me and understanding my moments of solitude and frustration when the investigation did not take the path that was supposed to go. Also, I want to thank my supervisor, Marcelo Segatto, and my co-supervisor, Maria Pontes, for guiding me at the right paths even when I haven't faith or failed to understand where my path was leading, without them I would not be here. I am also thankful to Diogo V. N. Coelho who first guided me in this jurney and was always there to answer my question even the silly ones. I am also grateful for all the assistance of Sabrina Feliz, Rosa Puentes and Breno Frizera, from the human resource team and the technical support from the laboratory that helped me with bureaucratic issues also when they help me to fix my computer, which decided to take a vocation in the middle of my studies. I am also very thankful for all my colleagues and friends that were also in the researching path giving me motivation to not give up because they already had passed through those moments that I was living. At last but not the least, I am really thankful for the National Council for scientific and technological development (CNPq - Conselho Nacional de Desenvolvimento Científico e Tecnológico) organisation also to the Espirito-Santence technology foundation (FEST - Fundação Espírito-Santense de Tecnologia) organization, as those were responsible for providing financial support for this Marter's thesis to be completed.

"A new commandment I give unto you, That ye love one another;
as I have loved you, that ye also love one another.
By this shall all men know that ye are my disciples,
if ye have love one to another".
(Holly Bible, John 13, 34:35)

Abstract

Over the year the demand for fast connections and the capacity to transmit great loads of data is one argument responsible for driving the development of new technologies and techniques to enhance the actual telecommunications networks. This work focused on studying the effects of applying an all-optical orthogonal frequency division multiplexing (AO-OFDM) process on passive optical networks (PON) for the next generation of telecommunications systems. The PON has been pointed as one solution to address the growing demand of the fast and bandwidth-hungry applications and services which are emerging from the advent of the 5G and the ever-growing popularity of smart devices. This work has shown that changing the Fourier transforms from the electrical to the optical domain not only avoid a significant data flow bottleneck, also that it is possible to enhance the actual grid further. This research had shown that it is possible to transmit over 1.28 Tbps over 90 km of standard single mode fibre (SSMF) or even it is possible to transmit over 640 Gbps over 240 km of SSMF, without any active device to amplify or repeat the signal.

Additionally, aiming to minimise the number of active devices used by placing an optical flat comb (OFC) source to generate multiple wavelengths from a single continuous wave (CW) light source. The OFC is based on the recirculating frequency shifting (RFS), from which this work achieve the generation of over 128 new wavelengths timely stable and with a power peak difference of 0.3 dB. Thus, this work had shown one possible scenario where a PON was applied with OFC generating 128 optical channels, where each channel was capable of transmitting 12.5 giga-symbols per second over 240 km of SSMF.

Keywords: All-optical, OFDM, OFCS, RFS, NG-PON, PAM-4.

List of Figures

List of Tables

List of abbreviations and acronyms

5G: Fifth-Generation

ADC: Analog to digital converter

AO-OFDM: All-optical orthogonal frequency division multiplexing

BER: Bit error rate

PC: Polarisation controller

CW: Continous wave

DD-MZM: Dual-drive Mach-Zehnder modulator

DI: Delay interferometer

DPSK: Differential phase-shift keying

DQPSK: Differential quadrature phase-shift keying

EbN0: Energy bit per noise density

FDM: Frequency division multiplexing

FEC: Forward error correction

FFT: Fast Fourier transform

FT: Fourier transform

ICI: Inter-carrier interference

IFFT: Inverse fast Fourier transform

IFT: Inverse Fourier transform

IoT: Internet of things

IQ-MZM: Phase-quadrature Mach-Zehnder modulator

MZI: Mach-Zehnder interferometer

MZM: Mach-Zehnder modulator

NG-PON2: Next generation passive optical networks two

ODN: Optical distribution network

OFC: Optical flat comb

OFDM: Orthogonal frequency division multiplexing

OFFT: Optical fast Fourier transform

OIFFT: Optical inverse fast Fourier transform

OLT: Optical line terminal

ONU: Optical network unity

OOK: On-off keying

OSNR: Optical signal to noise ratio

PAM4: Pulse-amplitude modulation with 4 levels

PON: Passive optical networks

PRBS: Pseud random bit source

QAM: Quadrature amplitude modulation

QPSK: Quadrature phase shift keying

RF: Radio frequency

RX: Receptor

RZ: Returning to zero

SNR: Signal to noise ratio

SSMF: standard single mode fibre

TX: Transmitter

Vbias: Bias Voltage

List of symbols

ΔT	Pulse signal spreading
λ	wavelength
ν_g	Grup velocity
$\Delta\lambda$	Range of wavelengths
L	Fibre length
D	Disperssion
τ	Symbol period
π	Pi
κ	Coupling coefficient
β	Propagation constant
l	Coupling length
c	Speed of light
f	frequency

Contents

1 Introduction

Increase in mobile data traffic and the likely growth resulting from the deployment of the fifth generation of radio access networks has stimulated research in technologies to enable more transmission capacity. To explore this commercial opportunity, companies and research organisations are discussing the next steps that the market can take. One promising enabling technology is the passive optical networks (PON) emerged as a solution for providing large bandwidth and support the increased demand for communication services. It already had been consolidated as the backbone for a massive load of data transmission, and it is becoming more common to be closer to the end user as the need high-speed data transmission grows. In this context of converging and enabling technologies, this work studies a source to provide multiple frequency channels, Fourier transforms applied to quickly convert quantities from the optical domain to the frequency domain, and vice-versa, and the implementation of different modulation formats. A closer look at the actual market trend sheds light on this study motivation.

1.1 Motivation

The market and user's demands drive a significant part in technology development. It is evident when looking at the sky-high soaring demand for data transfer and bandwidth-hungry services [2, 3]. For instance, video data traffic compose more than half of all mobile-information traffic, especially due to the increasing number of smart devices [3]. As presented by CISCO [2], high-definition video streaming, cloud storage and cloud computing are more common and predicted to increase shortly. It is not a surprise that smartphones and Television will compose more than half of all IP traffic as shown in Fig. 1. Moreover, all this data will converge for mobile phone cells hence optical networks would be used to transport all this information efficiently [4].

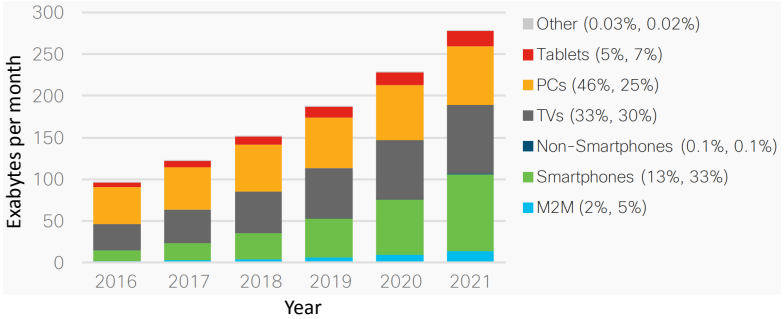

Figure 1 – Devices IP traffic share from 2016 to 2021, CISCO [1].

.

Technology must be ahead of the current demand although it seems not to be possible that a telecommunication system can catch up this ever growing trend. Without mention the constant growth of new technologies emerging from this new era such as the internet of things (IoT), which means that a miscellany of devices communicating with one another. Those communications commonly referred as machine to machine and the literature predict that those data flows will demand more from the network on flexibility, reachability and resilience [5].

One can notice that the concept of smart houses is becoming more realistic when one look at the IoT concept. Also, new devices such as 4K HD television are more common hence bringing about more consumers to hire data packages with higher bandwidth connection, which can fund an answer at passive optical networks (PON). That is also the bases for modern systems of fibre to the home [4, 6], due to its simplicity and lower cost if compared to a network that deploys active devices. Moreover, the exponential increase in mobile data traffic, as previously mentioned, even more with the upcoming deployment of the fifth-generation (5G) of radio access networks request more capacity from cell mobile backhauls [4].

Besides, the next generation PONs (NG-PONs) are also pointed as solutions for the mobile front haul, whose implementation improved intercell communications and allowed equipment downsizing of cellular networks [7]. At NG-PONs architecture, part of the operational base is moved closer to the remote antenna site, where an optical link is used for connections, the remote station will regularly require high bandwidth and resilience, which can be achieved with PON systems. Although, the actual network may not be able to supply enough resource for the real growing demand. Thus, more study and development concerning NG-PONs are in progress [4, 7]. Albeit, it was recently standardised, but not fully deployed, NG-PON allowing 10 Gbps aggregate symbol rate over 20 km covering up to 128 optical network unities (ONUs) under time-wave division multiplexing setup. Higher capacity will be demanded from the network. As a result, the institute of electrical and electronics engineers (IEEE) task force is working to standardise future PON able to offer 100Gbps (100G-PON) and aiming for the next generation of services and application demand [8].

1.1.1 Objectives

This dissertation aims to evaluate different techniques such as a variety of modulation formats, selection of channels through ideal filters and set of optical devices, various forms of generating multiple wavelengths from a single laser source, all those techniques will be used within a passive optical network ecosystem. We are exploring the benefits and drawback of each method and its applicability to an all-optical orthogonal frequency division multiplexing (AO-OFDM) architecture.

This work specific goal is to evaluate an AO-OFDM architecture capacity, and reachability can be significantly enhanced when used appropriated techniques. Then, this work aimed to propose the best approach fitted magnify an AO-OFDM PON efficiency usage regarding reachability and capacity.

1.2 Passive optical networks

Transmission of information through glass is not a recent idea however just after a breakthrough in glass fibre production in 1968 [9] this field has been experienced a significant growth mainly due to the optical fibre reachabilities, broad bandwidth capability and other features offered by this transmission medium. Thus, it is not by any surprise that the optical fibre has been motivating significant works in the optical systems field [10, 11, 12].

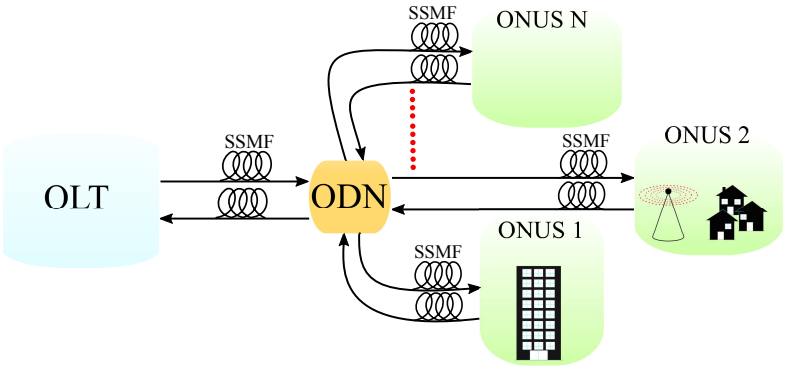

Figure 2 – Example of basic PON diagram.

Passive optical networks were being consolidated as the optical backbone approached and recently as the technology price decreases it became closer to the end user as shown in Fig. 2. Passive optical networks are mainly composed of three distinct elements the optical line terminal (OLT), the optical distribution network (ODN) unit and the optical network unit (ONU).

The OLT is located at a central office which has the primary responsibility of controlling, on the ODN, the data flow which may happen in two directions, downstream and upstream. The ODN is a significant component on the network which has the goal of redirecting the OLT signal to the correct ONU. Finally, the ONU is the final user or users relying on services on demand. At the ONU, the information is converted from the optical domain to the electrical domain and vice-versa. Since the optical domain has a broader bandwidth than the electrical domain, a higher number of final users can be connected to the same optical fiber to use its available bandwidth efficiently.

1.3 Development on optical networks

Regarding the evolution involving technologies implemented in optical networks, studies show that it is possible to reach even further transmission capabilities of a passive optical network as exemplified in Fig. 2. For instance, experiments were able to demonstrate four-channels 25-Gb/s per channel hence an overall of 100 Gb/s over 1 km of standard single mode fibre (SSMF) without optical amplifiers and less than eleven feed forward equaliser at the reception [13]. It was designed to create a PON for Data Center interconnectivity, and the development of pulse amplitude modulation achieved it with four amplitude levels (PAM4) transceiver for data rate. Although, the low cost and the high symbol rate capabilities, the electronic complexity was increased and this system can cover just its vicinity which is a maximum radius of 1 km.

Another example was the first real-time 400 Gb/s transmission over 100 km [14], designed to interconnect separated Data Centers. It was feasible by eight carriers at 50 G baud each divided into two groups, odd and even, where each group was modulated with PAM4 and combined by a 50 GHz interleaver, using optical amplifiers to ensure the correct power level would be received.

Besides, schemes for enhancing key points of long reach PON have been demonstrated such as coherent optical interleaved single-carrier frequency division multiplex, for optimisation for the uplink. As a result, a peak-to-average power ratio of 0 dB and ≈ 4.5 dB were achieved for a quadrature phase shift keying (QPSK) and 16 quadrature amplitude modulation (QAM), respectively. Nevertheless, a significant cost due to increased computational complexity was observed.

Besides the increase in reachability, it is also desired methods that diminish data flow barriers [15] exemplified by the optical fast Fourier transform (OFFT) implementation which transfers some electrical complexity to the optical domain. Bearing in mind that electronic circuits, even more, high-frequency circuits, are the bottleneck at the reception mainly due to the acquisition time of analogue to digital converters (ADC) beyond the buffering process needed. It is well known that by applying the OFFT at optical domain mitigate this issue as well as increases symbol rate capability. It was demonstrated [16] that is possible to achieve 640 Gbps using OFDM signal. The OFFT implemented in [16] was sensible to polarisation, and a mode-locked laser used as a synchronous controller in all stages of this process. Hence its complexity at the optical domain was increased.

Despite all enhancement that can be achieved, one should bear in mind that the NG-PON development must undergo knowing the long lifespan of optical networks and it has a high deployment cost. Therefore, new technologies and methods must coexist with the current technology allowing a more cost-attractive investment to be adopted by organisations in

the years to come [4, 6].

For those reasons, this work evaluated a proposed NG-PON2 architecture under different modulations formats aiming to demonstrate an optimal approach to apply our current technology. This thesis has achieved the symmetric symbol rate with 1.28 Tbps on downstream and upstream over 90 km of SSMF and even further 290 km with 640 Gbps. It can still be mentioned the high efficient bandwidth usage, which was granted by the all-optical OFDM signal used and a simplified and adaptative receptor, which implements the OFFT. Another feature its flexibility to respond to different user demands by combining on-off keying (OOK) and PAM4 techniques. The communication system considered in this work is discussed in the context of passive optical networks. The main structure of the optical line terminal (OLT) and optical network unit (ONU) that composes the PON is fed by a flat comb generator which from a single laser produces multiple wavelengths which is the core of this work once every new optical carrier must be orthogonal.

1.4 System requirements

This research was based on simulations focused on the physical layer of a PON system targeting to implement the Fourier transform at the optical domain as well as different modulation formats. Some constraints and assumptions were needed to build the simulation here created regarding the physical and practical limitations also the available resources. Thus, the devices here described were modelled from measured data acquired from laboratory experimentation or using general equations reported in the literature.

For instance, this work considered an SSMF with dispersion, attenuation and slope coefficients of 17 ps/nm x km, 0.275 dB/km, and 0.56 ps/nm^2 x km, respectively. Besides, the Mach-Zehnder modulator (MZM) modelling was obtained from experimental characterisation performed with the actual device LN86S-FC [17] hence allowing obtaining a realistic model for a dual-drive MZM (DD-MZM). This research also considered a continuous wave (CW) generated by a laser diode source at 1550 nm. Likewise, this work selected just 128 optical carriers due to computational limitations. Moreover, as dispersion is the main reachability and capability limitation of an optical system [18], another project constraint is better understood when one analysis the dispersion equation (1.1):

$$\Delta T = \frac{d}{d\lambda}\left(\frac{L}{\nu_g}\right)\Delta\lambda = DL\Delta\lambda, \tag{1.1}$$

where ΔT is the pulse signal spreading, D is the fibre dispersion, L is the fiber length, ν_g is the group velocity, $\Delta\lambda$ is the range of wavelengths, ΔT is the signal spread, directly proportional to the optical signal length and reverse proportional to the symbol period, τ,

as shown in (1.2)

$$\Delta\lambda \propto 1/\tau. \tag{1.2}$$

Therefore, the increment of τ causes the $\Delta\lambda$ to diminish proportionally, consequently ΔT also decrease due to dispersion. Thus, dispersion compensating fibre can be dismissed from the PON system using signals with relatively low baud rate, which is less affected by dispersion. As a result of this approach, controlling symbol rate can minimise system complexity inasmuch on all simulations the symbol rate was fixed as 12.5 Gbaud to avoid chromatic dispersion.

1.5 Dissertation Outline

This chapter gives an introduction on the importance of studying and developing methods about PON environment to address the sharp growth of the resources demand on telecommunication systems due to the arrival of new technologies such as 5G likewise the popularity of smart-phones as mentioned in 1.2. Similarly, this work had presented a brief explanation of a passive optical network and recent works searching on how to enhance it. Moreover, some project constraints were introduced to high light the simulation characteristics here developed as well as some limitations faced in this work. The following parts of this work were divided as follow. After the introduction chapter here described, secondly, it was presented the background chapter where the main principles associated with this work were discussed. Thirdly, the setup used was shown and its implementations described. Lastly, the results achieved and conclusion were discuses. The last chapter focused on evaluating the system under different scenarios to explore the best configuration for the system. Also, bringing about the procedures that had been done which are fundamental for this work conclusion. By the end of this thesis, it is expected to let clear the main accomplishments of this work which was the evaluation of optically implemented Fourier transforms applied on PON to enhance its capabilities. Also, this work proposed setup of the physical layer that takes in account different technologies such as the generation of multiple wavelengths, optical modulations and optical processing, noticing that those techniques haven't been evaluated in conjunct for the best of our knowledge.

2 Theoretical background

Before starting to argument on how to improve a PON system, first, it is essential to understand some underlying base principles such as ways to write information on a light beam and efficiently usage of available resources. Not only discussing some mathematical principles used on telecommunication but also exploring ways to implement them on the optical domain. Also, the description of the devices here used will be discussed just the essential that was considered to develop the simulations; other used components were deemed to be ideal. Moreover, all information here presented is general and can be applied in different areas. However, this work will focus on wavelength division multiplexing (WDM) systems since the optical networks evaluated are based on multiple wavelength principles.

2.1 Mach-Zehnder interferometer

Ludwig Zehnder proposed in 1891 a new interferometric setup to demonstrate the duality of the light [19], as a wave and as a particle. Shortly after, in 1892 Ludwig Mach refined the process [20] proposed by Zehnder resulting on the Mach-Zehnder interferometer (MZI). This experiment is shown in Fig. 3 and consists of splitting a light beam in two different paths with the same length.

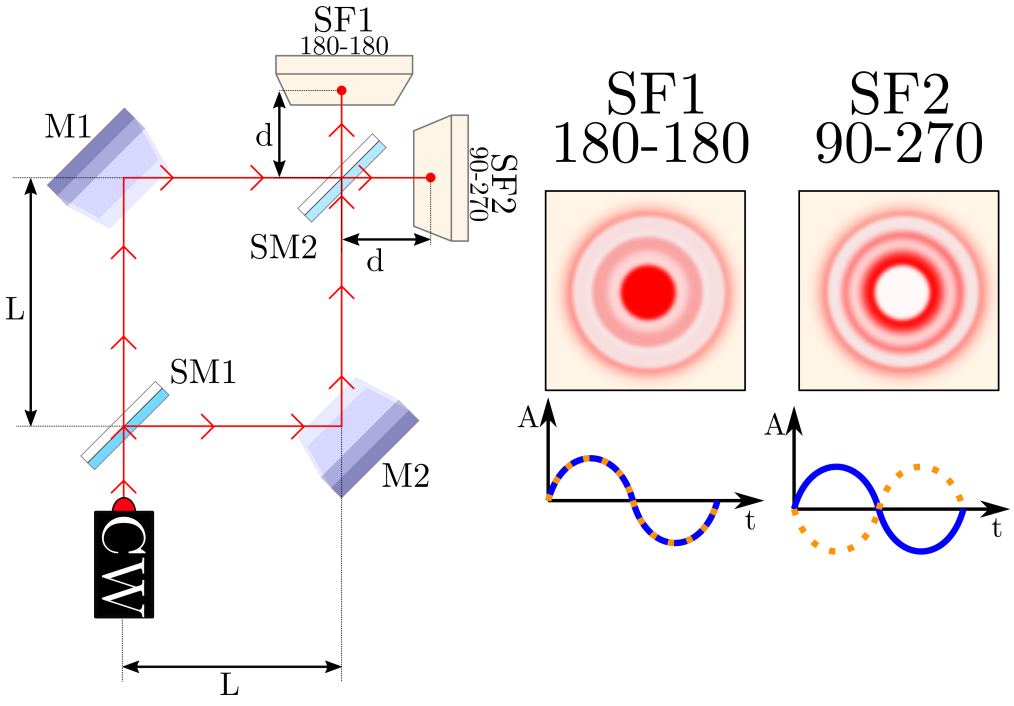

Figure 3 – Mach-Zehnder interferometer experiment.

To evaluate this experiment principle it possible to observe at first the semi-mirror (SM1) splits the light source, a continuous wave (CW) beam, equally into paths. One half is transmitted through SM1, the first path, the other half suffers a reflection of 90°. As a result, its phase is also added by 90°. Then, both light beams meet a mirror (M1 for the light at the first path and M2 for the light at the secondary path). Thus, both waves suffer a 90° reflection hence a phase offset of 90° was added. In the end, another semi mirror (SM2) further splits the incoming beam equally. Half of the light incoming from the first path is reflected towards the surface 1 (SF1) so gaining a phase offset of 90° and the other half is transmitted to the second surface (SF2). Similarly, half of the light incoming at SM2 from the second path is reflected towards the SF2 also gaining another phase offset of 90° and the other half is transmitted towards the SF1. Summarising, for each light reflection its phase is offset by 90°. The laser from the first path suffers two reflections before reach SF1, and one reflection before arriving at SF2. In contrast, the light on the second path undergoes two reflections before reach SF1 while suffering three reflections before hitting the SF2. Therefore, at SF1 there will be two laser beams arriving with the same phase offset whereas at SF2 there will be two laser beams coming with a phase difference of 180°. As a result, the light at SF1 will interfere with each other constructively whereas lights arriving at SF2 will interfere with each other destructively.

On the previous example, the light propagated through the air, although at optical devices the laser beam propagates, mainly, on crystals. Besides, some material under an electrical field can have its physical structure modified. Thus, this deformation also changes the crystal optical-electrical features. For instance, the susceptibility and permittivity of the material are altered due to an electrical field, and this effect is called the Pockels- or electro-optical Kerr effect [21]. As a result, the propagation index of a given structure can be controlled by an external voltage, therefore, altering the phase of a wavelength within it. Thus, combining those structures more complex optical devices can be built.

The MZI principle has been implemented on silicon devices. For instance, in Fig. 4a an illustration of a dual-drive Mach-Zehnder modulator (DD-MZM) is shown. The incoming CW at the DD-MZM is splitting into two paths, and a voltage on the DD-MZM electrical terminal is capable of changing its relative phase offset among pathways. Hence, an interferometric pattern will be built at the DD-MZM output. In other words, it is possible to control the CW intensity once the DD-MZM output is proportional to an applied voltage. Fig. 4b shows a Mach-Zehnder modulator (MZM) typical response, which is CW output intensity by polarisation voltage.

Furthermore in Fig. 4b, it is shown a constant voltage can set a working region for an MZM. Therefore, an alternate voltage can generate a variable output response. Summarising, an MZM can imprint electrical information into a light source.

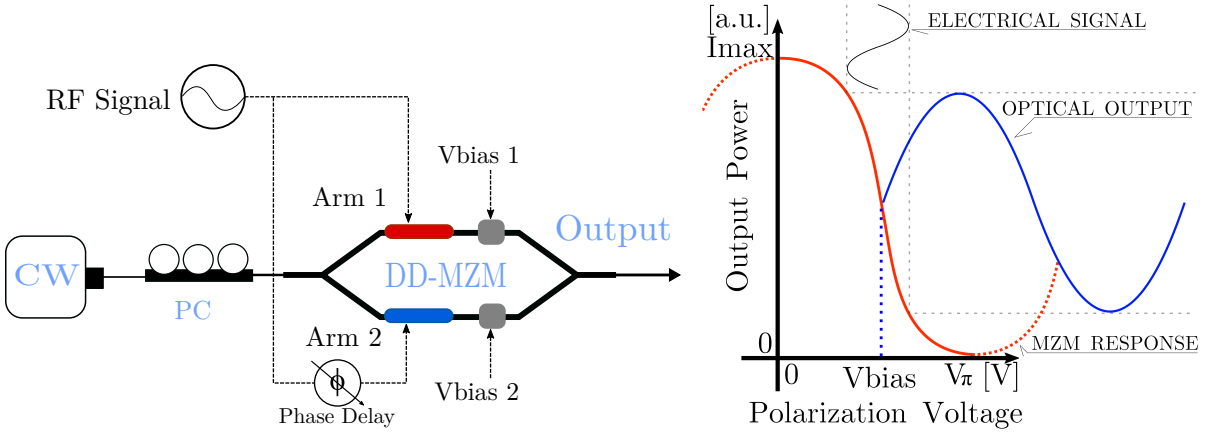

(a) Mach-Zehnder Modulator (b) Mach-Zehnder Intensity response

Figure 4 – Mach-Zehnder Modulator implemented in silicon divice on a) and its characteristic response on b).

The optical field at the DD-MZM output [22] can be expressed as eq. 2.1:

$$E_{out} = \frac{1}{2} E_{in} \left\{ e^{j\left[\pi \frac{V1(t))}{V_\pi}\right]} + e^{j\left[\pi \frac{V2(t))}{V_\pi}\right]} \right\}. \tag{2.1}$$

Where E_{out} is the optical field at the DD-MZM output, E_{in} is the optical field at DD-MZM input, $V1(t)$ and $V2(t)$ are the radio frequency (RF) signals at each arm of the modulator and V_π is the modulator characteristic voltage.

Moreover, $V1(t)$ and $V2(t)$ can be written as eq. 2.2 and eq. 2.3, respectively.

$$V1(t) = V_{b1} + cos(2\pi f_1 t) \tag{2.2}$$

$$V2(t) = V_{b2} + cos(2\pi f_2 t). \tag{2.3}$$

Where, V_{b1} and f_1 are the polarization voltage and the RF frequency, respectively, at DD-MZM first arm. Similarly, V_{b2} and f_2 are the polarization voltage and the RF frequency, respectively, at DD-MZM second arm.

Eq. 2.1 can be expanded as eq. 2.4:

$$E_{out} = \frac{1}{2}E_{in}\left\{cos\left[\pi\frac{V1(t)}{V_\pi}\right] + jsin\left[\pi\frac{V1(t)}{V_\pi}\right] + cos\left[\pi\frac{V2(t)}{V_\pi}\right] + jsin\left[\pi\frac{V2(t)}{V_\pi}\right]\right\} \quad (2.4)$$

Now, remembering some trigonometric proprieties such as:

$$cos(a+b) = cos(a).cos(b) - sin(a).sin(b) \quad (2.5)$$

$$cos(a-b) = cos(a).cos(b) + sin(a).sin(b). \quad (2.6)$$

Therefore,

$$cos(a+b) + cos(a-b) = 2.cos(a).cos(b). \quad (2.7)$$

Be it,

$$a + b = A \quad (2.8)$$

also

$$a - b = B. \quad (2.9)$$

Thus,

$$a = \frac{A+B}{2} \quad (2.10)$$

and

$$b = \frac{A-B}{2}. \quad (2.11)$$

Hence, replacing eq. 2.8 and eq. 2.9 into eq. 2.10 and eq. 2.11 results in eq. 2.12:

$$cos(A) + cos(B) = 2.cos\left(\frac{A+B}{2}\right).cos\left(\frac{A-B}{2}\right). \quad (2.12)$$

Similarly, eq. 2.13:

$$sen(A) + sin(B) = 2.sin\left(\frac{A+B}{2}\right).cos\left(\frac{A-B}{2}\right). \quad (2.13)$$

Thus, making $A = V1(t)$ and $B = V2(t)$ it is possible to re-write eq. 2.4 as:

$$E_{out} = \frac{1}{2}E_{in}\left\{2cos\left[\frac{\pi(V1(t)+V2(t))}{2V_\pi}\right]cos\left[\frac{\pi\,(V1(t)-V2(t))}{2V_\pi}\right] + j2sin\left[\frac{\pi\,(V1(t)+V2(t))}{2V_\pi}\right]cos\left[\frac{\pi\,(V1(t)-V2(t))}{2V_\pi}\right]\right\}$$

$$E_{out} = \frac{1}{2}E_{in}2cos\left[\frac{\pi\,(V1(t)-V2(t))}{2V_\pi}\right]\left\{cos\left[\frac{\pi\,(V1(t)+V2(t))}{2V_\pi}\right] + jsin\left[\frac{\pi\,(V1(t)+V2(t))}{2V_\pi}\right]\right\}.$$

Finally, the optical field at the DD-MZM output can also be expressed as eq. 2.14:

$$E_{out} = E_{in}cos\left[\frac{\pi}{2V_\pi}\,(V1(t)-V2(t))\right]e^{j\left[\frac{\pi}{2V_\pi}(V1(t)+V2(t))\right]}. \tag{2.14}$$

Hence, eq. 2.14 shows the output field as a product of three distinct terms: the incoming optical field, a cosinusoidal component responsible for modulating the incoming light and finally an exponential part representing the chirp effect. As $V1(t)$ and $V2(t)$ are also periodic, a solution for this equation can be found by Bessel series allowing the perception of multiples frequencies present at the DD-MZM output field [22].

Moreover, different modulation formats can be achieved with different points of polarisation. For instance, by setting a bias voltage (Vbias) at half of MZM characteristic voltage (V_π), the MZM will be polarised on amplitude modulation format whereas when Vbias is set as zero, the MZM will be polarised on a phase modulation format, as shown in Fig. 5.

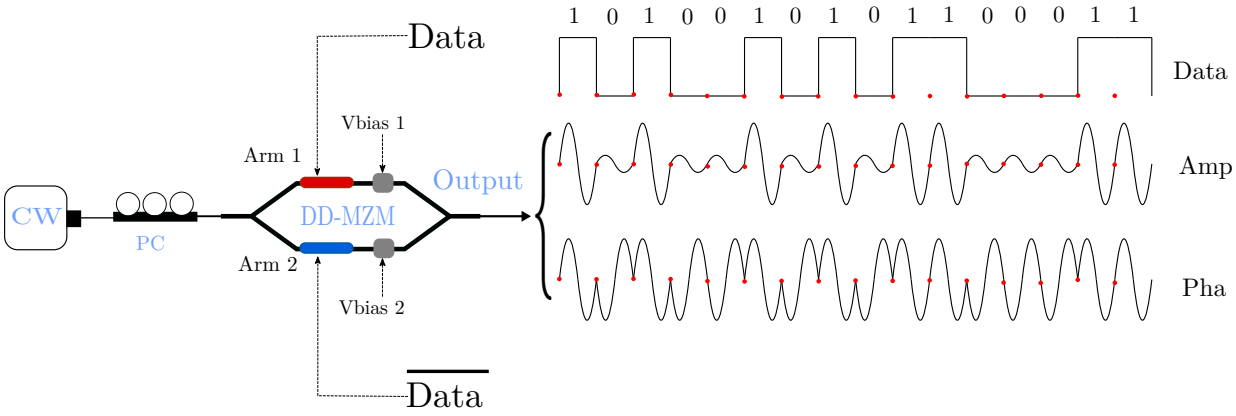

Figure 5 – Example of amplitude modulation and phase modulation implemented by a Mach-Zehnder.

2.2 Recirculating Frequency Shifting towards an OFC

Applying an optical flat comb source (OFC) on optical communication is desirable as the total amount of components used can be reduced, especially when a large number of optical carriers are needed. Thus, the existence of a myriad of studies and developments in this area is not a surprise [23]. Among all OFC generation methods, one can select the recirculating frequency shift (RFS) approach due to its time stability while the dual-drive MZM (DD-MZM) was chosen due to its capability of generating multiple carriers [24].

In the generated RFS setup, shown in the fig. 6, first of all, the incoming light passes through a polarisation controller (PC) selecting just one polarisation that maximises the MZM power output. Then, the light goes through the 3 dB optical coupler (OC), which sends half of CW power to RFS output, and the other half is sent to the optical ring. The DD-MZM, configured to operate as a single sideband suppressed carrier (SSB-SC), modulates the light with a radio frequency (RF) signal at 12.5 GHz. This activity does the modulator offsets the continuous wave (CW) by the RF signal. Then, the OC also sends half of the modulated light to RFS output while the other half re-enter on the optical ring alongside with the new incoming unmodulated CW. The optical amplifier (OA), positioned within the optical ring, compensates existent losses. Besides, the optical band-pass filter (BPF) constraint the number of generated carriers, as shown in Fig. 6.

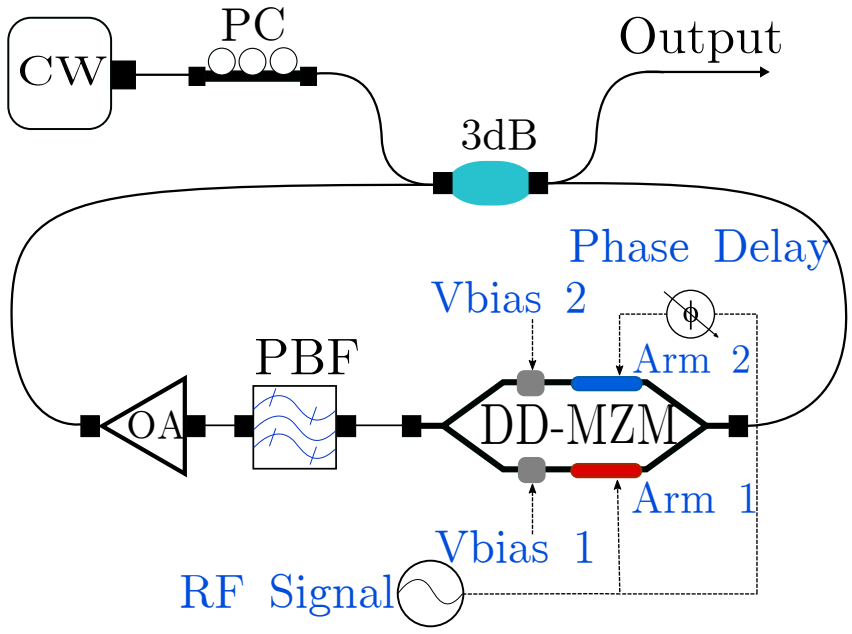

Figure 6 – Recirculating frequency shifting scheme (RFS).

The actual optical flat comb generated by the RFS process is further shown in the results chapter, once this section was responsible only to describe the RFS technique.

2.3 Optical couplers

Whenever this work talks about optical interferometers, those devices were modelled considering the association of optical couplers. In practice, for a direct detection system either the optical implementation of the Fourier transforms, those setups are performed by assembling independent couplers and some phase or time delays. Thus, it is clear that the modelling and implementation of those devices will have significant relevance for the final results achieved from the interferometers here used.

Objectively, an optical coupler is responsible for optical networks to combine and split signals. At this work, all couplers used will be considered to have four ports, meaning that two input and two output ports, as shown in Fig. 7. Directional couplers consist of two waveguides placed near each other at some point resulting in light coupling from one path to another and vice versa. This respective signal coupling is exemplified at Fig. 7 by the colours arrows, where each output will present a combination of each input. The proportion and nature of this combination will depend on the construction of the optical coupler. For instance, this device can be designed to be selective in wavelength; in other words, a coupler can be built to block totally or to let pass a specific wavelength. For this work, the device modelled was considered not to be selective or to have a broad transmission range, a more detailed description of an optical coupler and interferometers can be found at Ramashuam book [25] chapter 3.

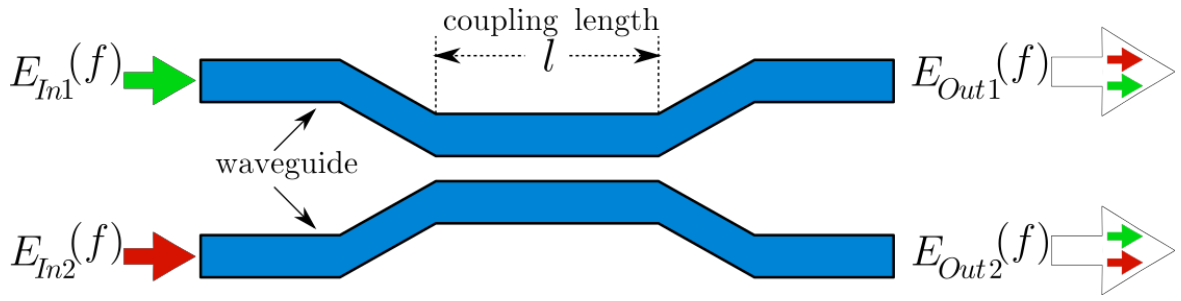

Figure 7 – Example of an optical coupler with four ports.

One approach to describe an optical coupler is through its equation, which is expressed by its output electrical fields $E_{Out1}(f)$ and $E_{Out2}(f)$. The output will be a combination of the input electrical fields,$E_{In1}(f)$ and $E_{In2}(f)$, by a matrix of transformation as shown in eq. 2.15 [25]:

$$\begin{bmatrix} E_{Out1}(f) \\ E_{Out2}(f) \end{bmatrix} = e^{-j\beta l} \begin{bmatrix} cos(\kappa l) & jsin(\kappa l) \\ jsin(\kappa l) & cos(\kappa l) \end{bmatrix} \begin{bmatrix} E_{In1}(f) \\ E_{In2}(f) \end{bmatrix} \tag{2.15}$$

where l is the coupling length, β is the propagation constant in each of the two waveguides of the directional coupler. The quantity κ is the coupling coefficient, and it is a function of

the width of the waveguides, the refractive indexes of the waveguiding region (core) and the substrate, and the proximity of the two waveguides [25].

2.4 Frequency division multiplexing

This section discusses the orthogonal frequency division multiplexing (OFDM) showing some of its implementation as well as a simple walk through its application. For a better understanding, this section will firstly bring a short introduction to the principles that allow light modulation. It is followed by an explanation about the frequency division multiplexing (FDM). Then, it is shown how the fast Fourier transform (FFT) and the fast inverse Fourier transform (IFFT) mathematical principles increases channel efficiency and capacity while mitigating interferences on the transmission process — this section ends by describing the implementation of the optical OFDM utilised in this work.

2.4.1 Seeking more efficient communication systems

Without noticing, we need to communicate mostly at every moment, be it by simple text messages, a phone call or contact the bank for some more specific details. No one would like to wait long periods for a connection to be established. Although, even without noticing, it is needed as we share mostly the same communication medium [26]. In contrast, at the beginning of telecommunications where each user had its physical channel, which was unused most of the time. Back then, the system was expensive, and a vast space was needed to deploy it. Soon, adding more users to the system could be more costly than what was charged. One walk around was to share the available resources among users, allocating one at the time accordingly. Even so, a different user would have different demands. Therefore, the medium-full capacity, such as its bandwidth was hardly used.

In a simple sense, the bandwidth is a range of frequencies that can be transmitted within a communication channel through a specific distance, the trapezium shown in Fig. 8. Thus, one can notice that beyond just allocating user within different time slots, which is commonly called as time division multiplexing (TDM), as accurately described at [27]. It is also possible to allocate multiple users in different parts of its bandwidth at the same time, also shown in Fig. 8. In this case, each sub-band, or carrier, is characterized by one frequency component, similarly, this process is also known as frequency division multiplexing (FDM), as discussed at [27], and it is illustrated in Fig. 8.

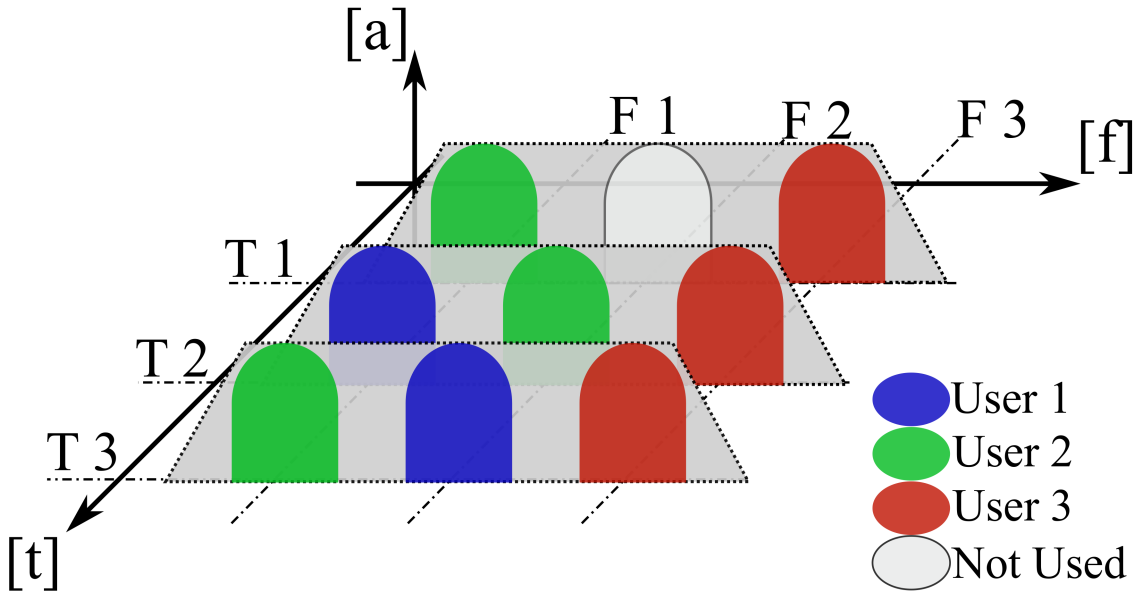

Figure 8 – Example of TDM and FDM process on channel bandwidth.

One can notice from Fig. 8 that the trapezium represents the available channel bandwidth. There, three different moments in time were selected to exemplify how three different users might be allocated. Firstly, if the channel has more capacity than the users require it, it can be divided into sub-band, or sub-channels, where a frequency, or carrier, will represent it. Here, three carries were selected, and for each one, a portion of the channel bandwidth was addressed. Even more, to avoid inter-carrier interference (ICI) a guard band was added among adjacent sub-channels. In other words, a small bandwidth slice must be placed between sub-bands to avoid further signal distortion. Thus, a user can load its information into a carrier, which may not be the same in different time slots.

Besides, the FDM process was also used in more complex systems, such as wireless communication. Knowing that the signal sent through the air may take different paths before it reaches the receptor, so each different path means a different time and phase delay of the incoming signal. Therefore, symbols arriving at a different moment will generate inter-symbolic interference (ISI), as shown in Fig. 9a, where τ represents a symbol period. Thus, the interference was mainly caused by the time that the signal arrives at the receptor when different paths are taken. Hence, one possible mitigation is to increase the symbol period where the maximum delay would fell in a small interval of the received signal, as shown in Fig.9b.

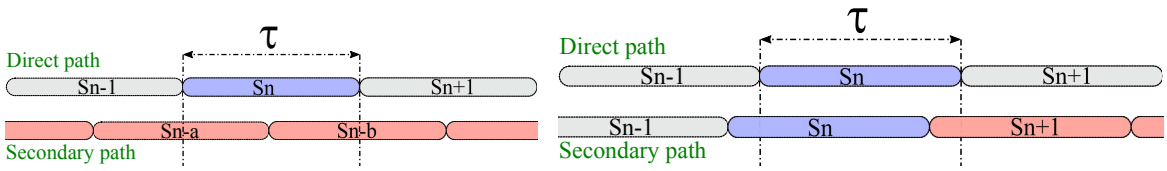

(a) Significant interference due path delay (b) Minor interference due path delay

Figure 9 – Inter-symbolic interference caused by the multiple paths that the signal can take until arrive at the receptor.

When the time delay is greater than half of the symbol period, the majority of the income information from the secondary path will interfere with the actual symbol on reception. One possible solution is to reduce the symbol rate until the maximum delay causes a minimum overlapping, as shown in Fig 9b. In other words, symbol rate reduction means increasing the symbol period thus limiting the maximum interference caused by secondary paths within a small part of the actual symbol. On the other hand, the transmitted symbol occupies less bandwidth as larger is its period hence there will be more free space to share among sub-carriers. [28, 29].

2.4.2 Orthogonal frequency division multiplexing

It should be noted, due to the ever-growing user resources demand every slice of channel bandwidth is valuable. Researchers aim to develop methods of placing sub-channels as close as possible to avoid guard bands usage. The OFDM is one example of multi-carrier transmission approach, which is a variant of the FDM, able to place multiple carriers side by side without guard bands. Besides, it is possible to improve, theoretically, in 50 per cent the spectral efficiency [30] with this method, as displayed in Fig. 10.

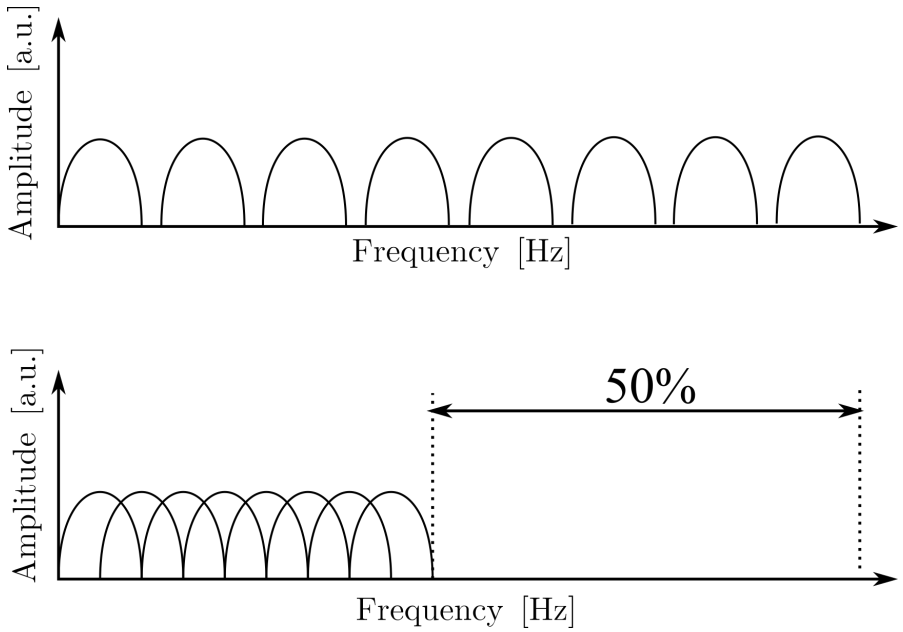

Figure 10 – Example of bandwidth efficiency enhancement by using an OFDM signal.

In 1966 with the pioneering work of Robert W. Chang the first OFDM scheme was presented [31]. This process places sub-carriers overlapping each other. Albeit not randomly, some criteria must be met such as equally spaced and with equal signal power aiming to grant carriers their orthogonality. Orthogonal signals have the characteristic of their inner product to be zero, which allow mathematical tools such as IFFT/FFT multiplex and demultiplex, respectively, the transmitted information at the frequency domain.

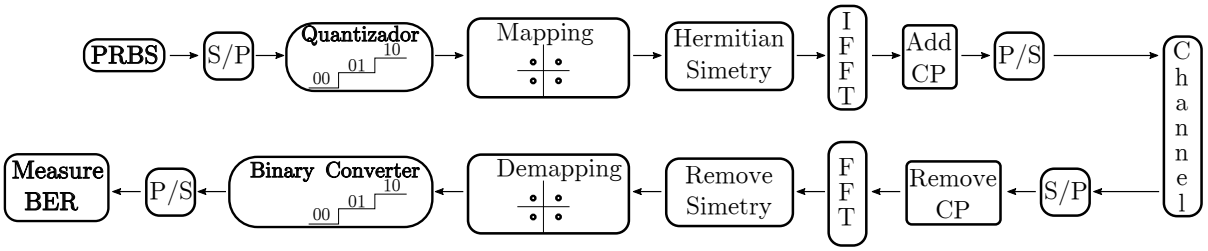

Figure 11 – Symple OFDM system block diagram.

Fig. 11 shows a simple OFDM transmission and reception set up. This set up takes a random serial bit stream and convert to parallel. Then, a group of bits are converted to

different levels before being mapped by a modulation process such as quadrature amplitude modulation (QAM) or a phase shift keying. Then, the signal receives a Hermitian symmetry. Following, each message is multiplexed by the IFFT process. In the end, the cyclic prefix (CP) is added before the signal be converted to a serial sequence to be transmitted through a channel. At the reception all steps early implemented are removed in the reverse orders. Highlighting the IFFT and the FFT as the main blocks in the transmission and reception process [28], respectively. Also, the fast Fourier transform is very important for engineering and others science fields.

For a time-discrete system the FFT is driven from the actual Fourier transform (FT), which can be mathematically written as the eq. 2.16:

$$X_k = \frac{1}{\sqrt{N}} \sum_{m=0}^{N-1} x_m \exp\left(\frac{-j2\pi km}{N}\right) \qquad for \;\; 0 \leq k \leq N-1. \tag{2.16}$$

Additionally, the inverse fast Fourier transform (IFFT) is also driven from the actual inverse Fourier transform (IFT), that can be written as Eq. 2.17:

$$x_m = \frac{1}{\sqrt{N}} \sum_{k=0}^{N-1} X_k \exp\left(\frac{j2\pi km}{N}\right) \qquad for \;\; 0 \leq m \leq N-1. \tag{2.17}$$

Where X_k is a frequency component, N is the number of FT/IFT points, m is the sample index, k is the frequency index and x_m is the time sample.

A more realistic view of how the FT/IFT implemented is shown in the butterfly diagram from which the actual FFT/IFFT used in this work was implemented, Fig. 12. There, it was represented an FFT of eight points. The time samples x_n at the left side are the inputs on this process and combined as displayed by the arrows. One can notice the multiplexing process, of all inputs to all output frequencies, highlights how each frequency component has a contribution from all input samples. As a result, the signal at the frequency domain was obtained on the right side of the diagram, Fig. 12. The reverse process can be done by following the same diagram although from right to left and now using W_n^{-k}, which is $\exp\left(\frac{j2\pi km}{N}\right)$. Hence the sing of k is modified to implement the FFT or the IFFT.

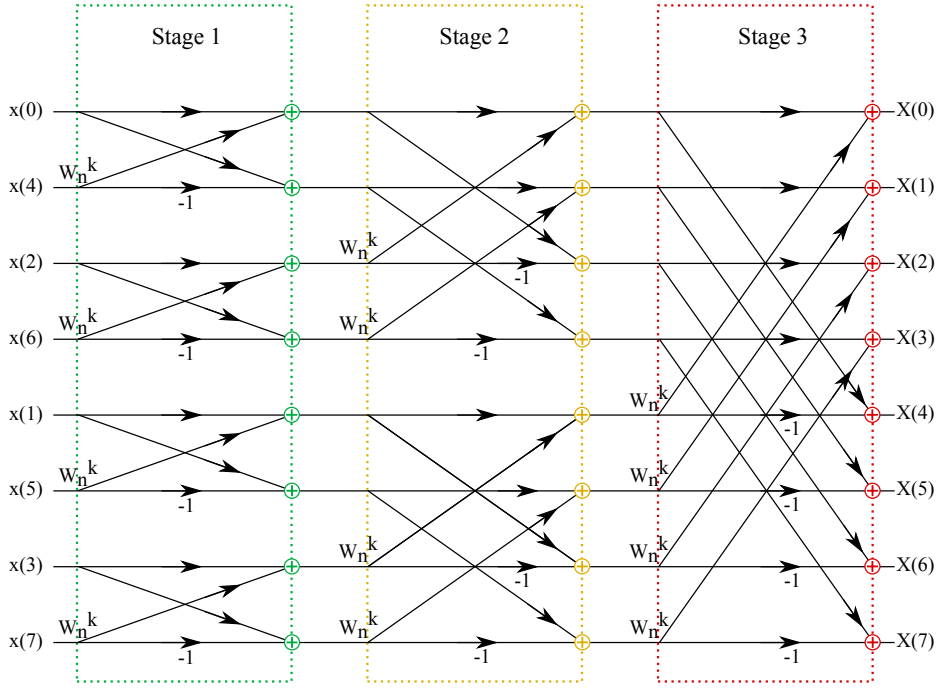

Figure 12 – FFT butterfly diagram.

From Fig. 12, it is clear how a signal at time domain can be expressed as a combination of multiple frequencies. Thus, placing symbols to be transported by a set of frequency carriers X_k the IFFT process multiplex all carriers to compose an OFDM signal at time domain to be transmitted as shown in Fig. 6. Similarly, at the receptor, taking samples of the OFDM signal is possible to recover the transmitted carriers through the FFT process hence demultiplexing the symbols previously sent.

The transmission process may disturb the signal orthogonality, which is vital for the Fourier transform [29, 32]. Disturbances cannot be avoided entirely on actual systems, which are mainly due to the transmission channel. Effects of interference commonly observed are inter symbolic interference (ISI) and inter-carrier interferences (ICI) [28]. The ISI is mostly due to the multipath channel characteristic where the signal arrives at the receptor in different time slots. One example of ICI happens on optical fibre propagation due to the signal spread within the optical medium.

Multipath interference can be mitigated by adding a cyclic prefix (CP) and increasing the OFDM symbol period to be higher than the most extended significant path delay. The CP is a redundancy created by copping a beginning portion of the OFDM signal and placing it at the end of the OFDM symbol. Thus, the signal incoming on a secondary path will fall within the CP portion. In other words, the actual symbol period (Ts) will be the time used (Tu) of the symbol added the time of guard (Tg) of the symbol ($Ts = Tu + Tg$). In fact, this process was developed to increase the symbol period by a percentage, which was precisely the same approach to avoid fading due to multi-paths in a transmission system previously mentioned.

2.4.3 FFT Optical Implementation

The optical implementation of the FFT can be exemplified by the transmission of an arbitrary signal as shown in Fig. 13a. Once, the Fourier process allows us to transmit multiple pieces of information at the same time, here the signal was sampled four-times per symbol period. Thus, a four points FFT will be used in this example as shown in Fig. 13a, which represents the schematic of a traditional electrical FFT.

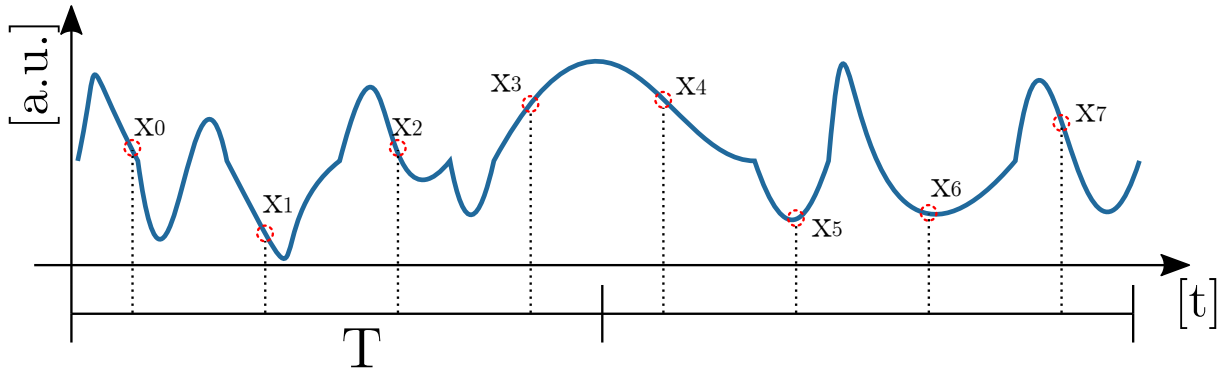

(a) Arbitrary signal to be transmitted by the FFT process.

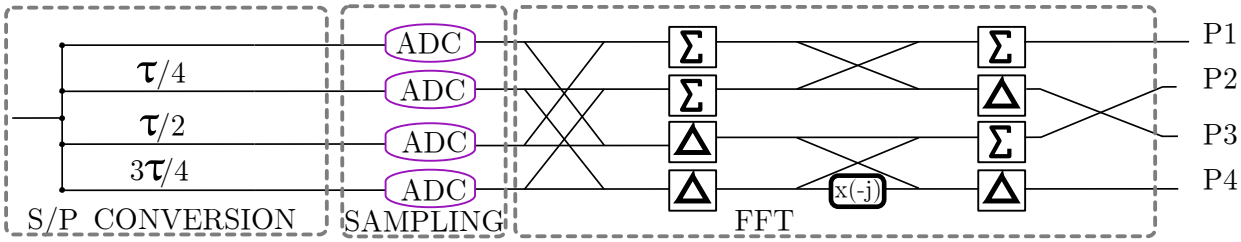

(b) Electronic implemented FFT process of four points.

Figure 13 – Example of the 4 point FFT implementation, shown in b), of a signal with an arbitrary amplitude in the function of time as shown in a).

The optical implementation of the electrical FFT was proposed by [33], and it is shown on Fig. 14. On this first implementation, it used simple directional two-input two-output optical couplers with other passive elements such as delay line and phase delay. Moreover, the simplification of this setup was proposed by [34], which consist of rearranging the devices to avoid redundancies and additional components.

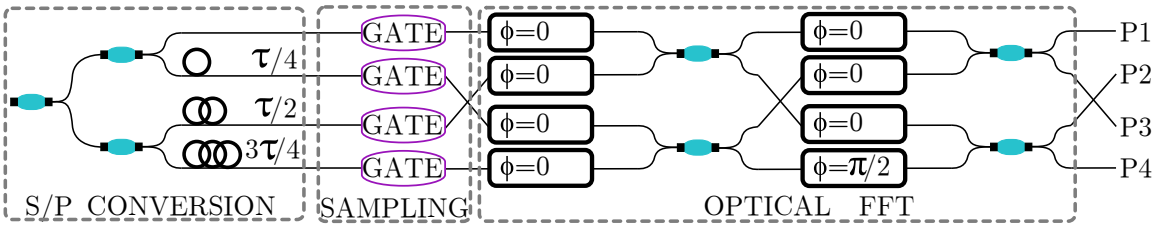

Figure 14 – Optical equivalent process for the traditional electronic.

The first step is to reorder some devices to diminish cross-paths and to place similar components together. As shown in Fig. 15, the one-quarter time delay was set with the three-quarters delay because they can be simplified. As a result gate at output 2 and 3 must be reordered as well because the order of the FFT process changed.

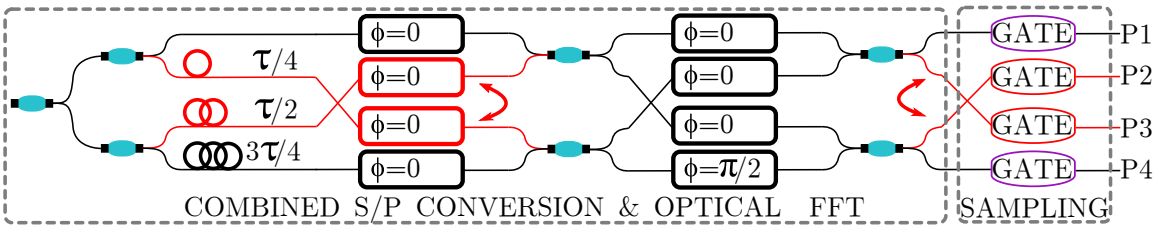

Figure 15 – Rearranging components to minimize path crossing on the optical FFT process.

Secondly, the one-quarter delay can be put in evidence, from the up arm at the bottom and the lower arm with three-quarters delay, also it can move forward on the diagram, as shown in Fig 16. Thus, just two types of time delay devices were needed hence a small simplification is already set.

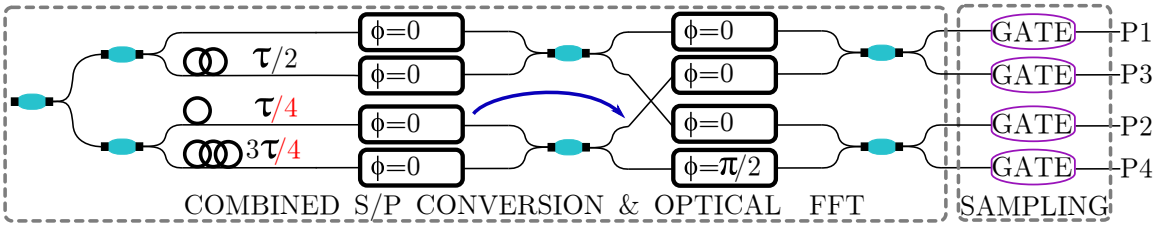

Figure 16 – Moving the common time delay forward on the diagram to simplify the optical FFT process.

As a result, at the beginning of the optical FFT diagram, there are repeated elements which can be further simplified by merging them and adding a coupler after them to share its signal between the following paths, as shown in Fig 17.

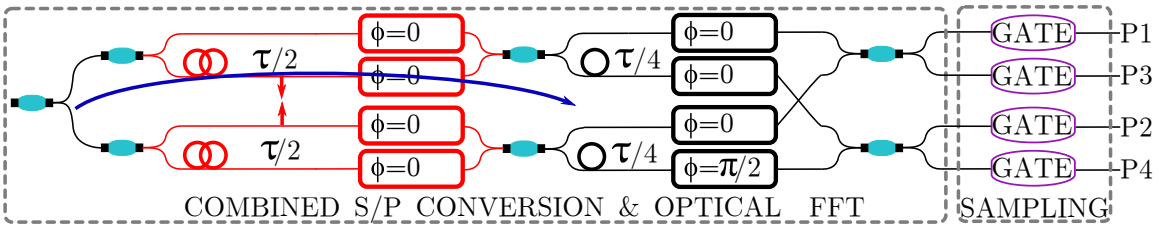

Figure 17 – Eliminating repetitions and splitting common signals to simplify the optical FFT process.

Finally, as shown in Fig. 18, it was possible to achieve our final and simplified diagram that uses fewer components and allows better scalation if needed. The complete mathematical description of this implementation is further demonstrated in [34]. From this approach, this work construct models for the devices here used to build the flexible optical FFT device based on cascade Mach-Zehnder interferometers, as one may notice at the output of each optical coupler there will be the constructive and destructive interaction of the incoming light, which math the description of an MZI, as previously described.

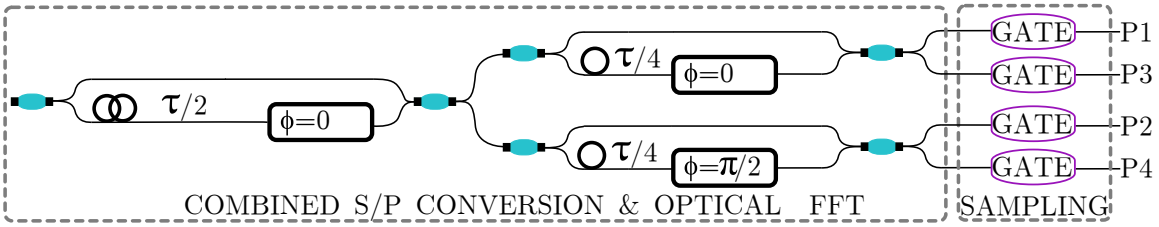

Figure 18 – Final 4 point optical FFT process equivalent to the traditional electrical implementation.

2.5 Modulation and mapping formats

There are two forms of transmitting a new piece of information. Firstly, a signal can be sent as precisely as it is, aiming to preserve its original characteristics which process is the analogic transmission. Although analogic communication is more straightforward and can provide more fidelity of the received signal to the transmitted information, the analogue signal is very susceptible to interferences. Digital transmission is another possibility of sending information with more resilience to interruptions. The data is first converted to the digital domain, losing some precision, then it can be processed before transmission. The signal sent through a medium is always analogic although in a digital process this signal is representing symbols which are equivalent to bits. Thus, they are less complicated and can be predicted whereas as an analogue image, for example, is cumbersome and hard to be predicted [35].

Once a piece of information is created, for instance when recording a video, and its data is ready to be sent, this information is not yet prepared to be transported by a medium. Firstly, the data needs to be adjusted by a modulation process accordingly to a transmission media such as open air, optical fibre or a metallic cable. For example, if in a video transmission we want to send one block per second and each block has 120 images, and each image is represented by 104 bits. Thus, we are transmitting roughly 12.5 kilobits per second (kbps). Therefore, the transmitted signal will have 12.5 kHz of frequency. Through the air, the receptor should have an antenna of one quarter the signal wavelength, which is approximately 24 km given by eq. 2.18. Hence, the antenna would be around 6 km of length, and this value is not practical. Now, if we modulate the signal, adjusting it to the air medium, by a carrier of 2.5 GHz, which correspond to a wavelength of approximately 0.12 m given by eq. 2.18. Thus, the receptor antenna should be around 30 mm, which is more practical. Therefore, modulation is essential to adjust the information to be transmitted accordingly with the telecommunication network media [35].

A signal wavelength is given by:

$$\lambda = \frac{c}{f} \tag{2.18}$$

where λ is the signal wavelength in meters, c is the speed of light in m/s and f is the signal frequency given in Hz unit.

Bit mapping and line coding are essential processes on the digital transmission to be implemented before the modulation. Bit mapping consists of techniques to increase the system bit rate and resilience. For instance, the differential phase shift keying (DPSK) is a one-bit mapping technique. The DPSK stores a bit on the carrier phase, hence making the signal more resilient to amplitude distortion. In contrast, the pulse amplitude modulation with four levels (PAM4) is a two-bits mapping technique storing two-bits information on the carrier amplitude level. Thus, one symbol PAM4 can transmit more information than a symbol DPSK. Besides, the line coding increases system transmission efficiency. For instance, return to zero (RZ), Manchester coding and the inverse Manchester coding can reduce low-frequency components, which can not be for long distances transmission, also enable the clock signal to recover.

This work selected the non return to zero line coding due to its simplicity, and the clock system can be related to the system bit rate. In contrast, the RZ and Manchester line coding, the clock must be at least the double of the system bit rate [35, 36]. A comparison among those line code formats with shown in Fig. 19.

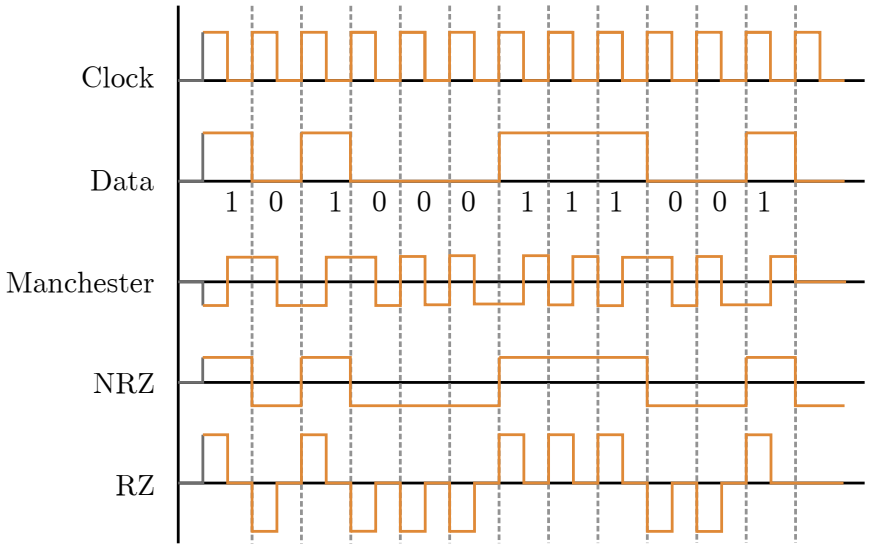

Figure 19 – Comparing data coding between Manchester, RZ and NRZ line code formats with bipolar signalling.

From Fig. 19 it is clear that when long sequences of ones or zeros occur the NRZ will present a high DC value, which is mitigated with the RZ and further minimised by the Manchester. Also, it also clear that despite the NRZ the other coding formats will require a higher sampling rate.

2.6 Signal-to-noise ratio

Communicating is to send and receive understandable pieces of information. In a telecommunication system, there are vast assortments of elements capable of interfering in the communication process. For instance, an analogue to digital conversion, the quantisation process may not represent the infinity of possible values of an analogue signal; hence this imprecision may cause problems at the receptor. Also, when multiple channels, or carriers, may interfere with each other resulting in possible issues at the reception. Moreover, temperature, vibration, amplification, and device proprieties add more interference on the information that has been transmitted. All those interferences and possible others can be seen as noise to the receptor [29, 28, 37].

An analogy can be found when we walk on a street talking with a friend. We try to understand the transmitted message. However, the sounds of cars, other people walking, construction sites, sirens, all those sources interfere in this process. Thus, we may not

distinguish all these sounds when we were focused on the speech as they represent just noise when compared with the information that we intend to decode.

It is clear that the information extraction from a transmitted signal is directly affected by all noises present on the system. Thus, one important parameter to evaluate a system performance is to measure the signal power to the noise power ratio (SNR) of a signal, which can be expressed as eq. 2.19 [37]:

$$SNR = \frac{Ps}{Pn} \tag{2.19}$$

where Ps is the signal power, and Pn is the noise power. Similarly, this equation can be written in decibel (dB) as eq. 2.20:

$$SNR_{dB} = Ps_{dBm} - Pn_{dBm} \tag{2.20}$$

where Ps_{dBm} is the signal power in dB, and Pn_{dBm} is the noise power in dB.

From eq. 2.20 it is possible to understand the SNR as a measure of distance as the difference of two points in a graph. In other words, it shows how a signal is far away from the noise. As an example, comparing with the analogy previously mentioned, a low SNR value would be like talking with a friend in a noisy street whereas a higher SNR would be like talking with a friend inside a quiet library. Therefore, the SNR can be used as a parameter to evaluate a system resilience to noise environments as well as to compare how different systems behave at the same levels of SNR.

To analyse the BER parameter on a simulated system is more common to use the energy bit per noise density (EbN0) because it is simpler to find the signal bit energy. Even more, there is a straight equation able to relate EbN0 to SNR. Firstly, it is important to relate EbN0 with energy symbol per noise density (EsN0) by the eq. 2.21 [38]:

$$EsN0(dB) = EbN0(dB) + 10log_{10}(k) \tag{2.21}$$

where k is the number of bits per symbol and a relation between EsN0 and SNR can be driven from eq. 2.22:

$$EsN0(dB) = 10log_{10}\left(\frac{Pin.T_{symb}}{N/B_n}\right)$$

$$EsN0(dB) = 10log_{10}\left[B_n.T_{symb}.\left(\frac{Pin}{N}\right)\right]$$

$$EsN0(dB) = 10log_{10}\left(B_n.T_{symb}\right) + SNR(dB) \tag{2.22}$$

where Pin is the effective signal imput power in watts, T_{symb} is the period of symbol, N is the noise power in watts and B_n is the noise bandwidth in hertz. Combining eq. 2.21 and eq. 2.22 is possible to achieve eq. 2.23:

$$SNR(dB) = EbN0(dB) + 10log_{10}\left(k\right) - 10log_{10}\left(B_n.T_{symb}\right) \tag{2.23}$$

then, one can notice that it is possible to relate EbN0 with SNR as a function of the noise bandwidth and the symbol period.

2.7 Optical signal-to-noise ratio

Indeed, there are a variety of interferences steeming from different natures [39]. On optical communication system, optical amplification plays a significant role in signals degradation [40] due to the amplified spontaneous emission (ASE). In fact, this signal abasement is quantified by a parameter Fn named amplified noise figure, which is given by the eq. 2.24:

$$Fn = \frac{SNR_{in}}{SNR_{out}}. \tag{2.24}$$

The SNR on eq. 2.24 is the electric power when the optical signal is converted to the electrical domain. The noise figure is an important parameter to show the quality of an erbium-doped fibre amplifier, for instance. The ideal value would be Fn equal to one once its value indicates how the signal SNR will diminish as a result of this amplification process. Also, the Fn cannot be smaller than one; otherwise the referred amplifier would be adding gain meanwhile removing noise from the signal.

In fact, to measure the optical signal to noise ratio (OSNR) is not an easy task. For instance, due to the broad spectrum of the glass fibre, it is hard to separate the signal and noise bandwidths. For historical reasons, a reference for bandwidth is commonly set to be 12.5 GHz as a result of the minimum resolutions of previous optical spectrum analysers (OSA) resolution. Moreover, there are many different proposals of how to efficiently measure the signal OSNR [41, 42] this work will use the method [37] based on the eq. 2.25:

$$OSNR = \frac{P}{2N_{ase}B_{ref}} \tag{2.25}$$

where P are the total average signal power added over two polarisation states, N_{ase} is the spectral density of amplified spontaneous emission accounted on one polarisation and

B_{ref} is the reference bandwidth. On this equation, the 2 factor is usually added because of the two polarisations from the ASE. It is possible to relate optical to electrical SNR by working on eq. 2.25. In fact, the OSNR differ from the SNR by a scalar factor, which depends on how the signal power is taken into account and the noise bandwidth assumed. Eq. 2.26 can be written as:

$$OSNR = \frac{pR_s}{2B_{ref}} SNR \tag{2.26}$$

where p is 1 when the signal has just one polarisation or 2 for two polarisations of the signal, R_s is the line signalling rate (symbols per second). Furthermore, this work will consider a signal with just one polarisation, reference bandwidth of 12.5 GHz. Also, all noise will be added only at the receptor after the photo-diode and will have a Gaussian distribution. In other words, the photodiode here is considered to be ideal as well as other devices here used such as optical coupler, filters and splitters hence adding noise on others parts would be difficult to measure, and the result would be coloured due to filters on the system. Thus, adding noise at the end of the system should be the option. Moreover, due to the usage of ideal components and the absence of noise, there is no meaning for discussing absolute power values since a signal with 0 dBm would have the same result as a signal with -30 dBm in our system. However, debating bout relative value is valid since the total losses in a system is known [43] as well as the minimum power needed at a photodiode to be detected [44].

To sum up, it was shown the theoretical embasement to assist on the understanding of upcoming chapters. The basic principle of light modulation based on Mach-Zehnder was presented to gather with different modulation formats implemented with this device. Similarly, the optical implementation of mathematical methods was also shown which are responsible for improving system capacity and enhancing the efficient use of the available bandwidth. Finally, this chapter has shown how to relate OSNR, SNR and EbN0, which is essential to understand the results presented later on this dissertation.

3 PON setup under study and system's configurations

This chapter presents the main structure of the OLT and ONU that composes the communication system fed by a flat comb generator which produces multiple frequency carriers. Also, here is presented the steps and considerations used to implement the simulation setup of a PON physical layer. Special attention is given on two main points: the Fourier transforms applied at the optical domain and the implementation of different modulation formats.

A communication system structure as a passive optical network concept is shown in Fig. 20. The selected architecture that will be evaluated in this work will have three essential parts. The block known as optical line terminal (OLT) contains the elements that generate the frequency carriers for transmission. The optical flat comb (OFC) source is responsible for create, by the RFS process, the multiple wavelengths to be multiplexed in the OLT.

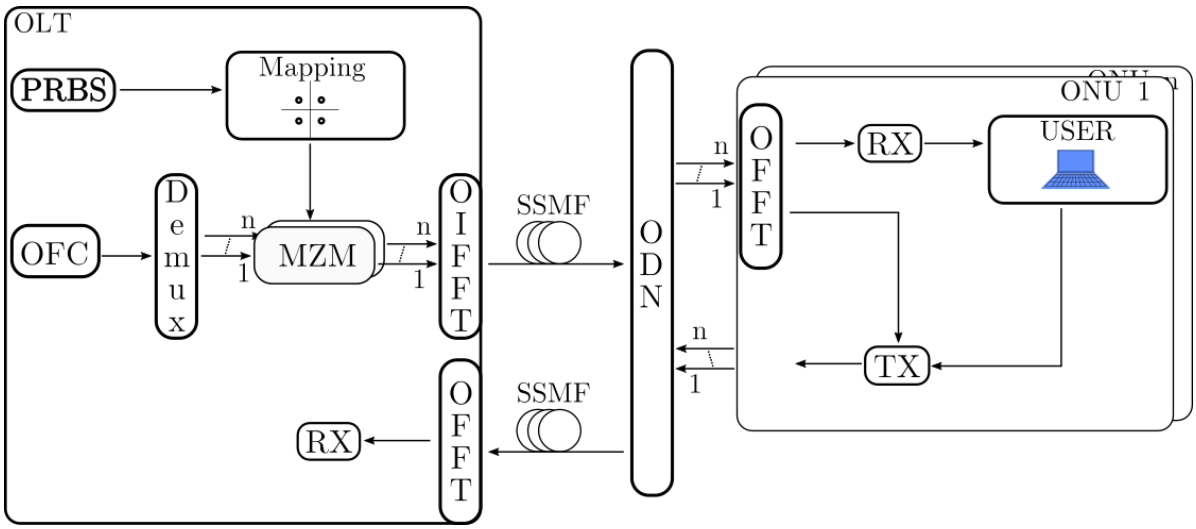

Figure 20 – Passive optical network (PON) setup under study based on all-optical orthogonal frequency division multiplexing (AO-OFDM).

Secondly, in the process to generate multiple optical carriers, the odd carriers are modulated for downlink transmission whereas even carriers are separated for the upstream propagation. Aiming to compose the various optical carriers maintaining properties of orthogonality for propagation, an OIFFT is accomplished in the OLT, that can multiplexes all parallel optical channels meanwhile preserving the orthogonality among carriers [45]. The OIFFT also avoids approximately 20 dB of crosstalk noise than a conventional optical combiner. In this case, each MZM output will go within optical couplers with N to 1 configuration

where N is the number of inputs of the coupler. The value of N can vary depending on is cascaded coupler were used a straight option would be N equal to 128.

The output form OIFFT is already the all-optical OFDM signal, and it is coupled to the optical fibre. The SSMF is coupled to an optical distribution network (ODN), which is responsible for splitting the optical carrier to several optical network units (ONU). When received at the receptor (RX), the OFFT is then responsible for demultiplexing the AO-OFDM signal selecting just carriers of interest.

In our architecture setup under evaluation, the optical amplification is performed only at the OFC block, a process which is located at the OLT. In other words, PON relies just on passive elements outside of the OLT, which means that no additional optical amplification was performed rather than at the RFS process. Therefore, the OFC generated must have enough power to be transmitted downstream as well as upstream.

On the following section of this chapter, each block will be explained with more detail about its functions and implementations for this setup.

3.1 Spliter and combiner steps

Telecommunication systems commonly use the OFDM technique, especially at wireless communication. As previously mentioned, the OFDM presents an efficient bandwidth usage also a high symbol rate capacity. However, under an infrastructure based only on electronic components can become a bottleneck on high-speed telecommunication systems such as a PON. As the IFFT/FFT process needs all samples to be processed at the same time, a buffer and time delays are required to store and synchronise, respectively, the data before processing it.

Therefore, from the setup earlier described, three blocks were implemented similarly: the Demux, OFFT and OIFFT blocks. All those blocks were implemented under the all-optical Fourier transforms approach. Where the Demux and OFFT blocks were responsible for splitting each optical channel into independent signals, and the OIFFT was responsible for combining all carriers accordingly. By applying this system at both ends of this system, the orthogonality of the system is preserved [34].

3.1.1 Optical inverse/fast Fourier transform

For the next PON generation, the IFFT/FFT process should be continuously and without delay. One approach is to implement the IFFT/FFT in the optical domain. The optical inverse Fourier transform (OIFFT), and the optical fast Fourier transform (OFFT) can be implemented with cascaded Mach-Zehnder interferometers (MZI) [34], as shown in Fig. 21. The cascaded MZI setup is a bidirectional process implementing the OFFT from left to right whereas the OIFFT is implemented from right to left. Moreover, this architecture naturally allows the serialisation and parallelisation to happen together with the Fourier transform processing.

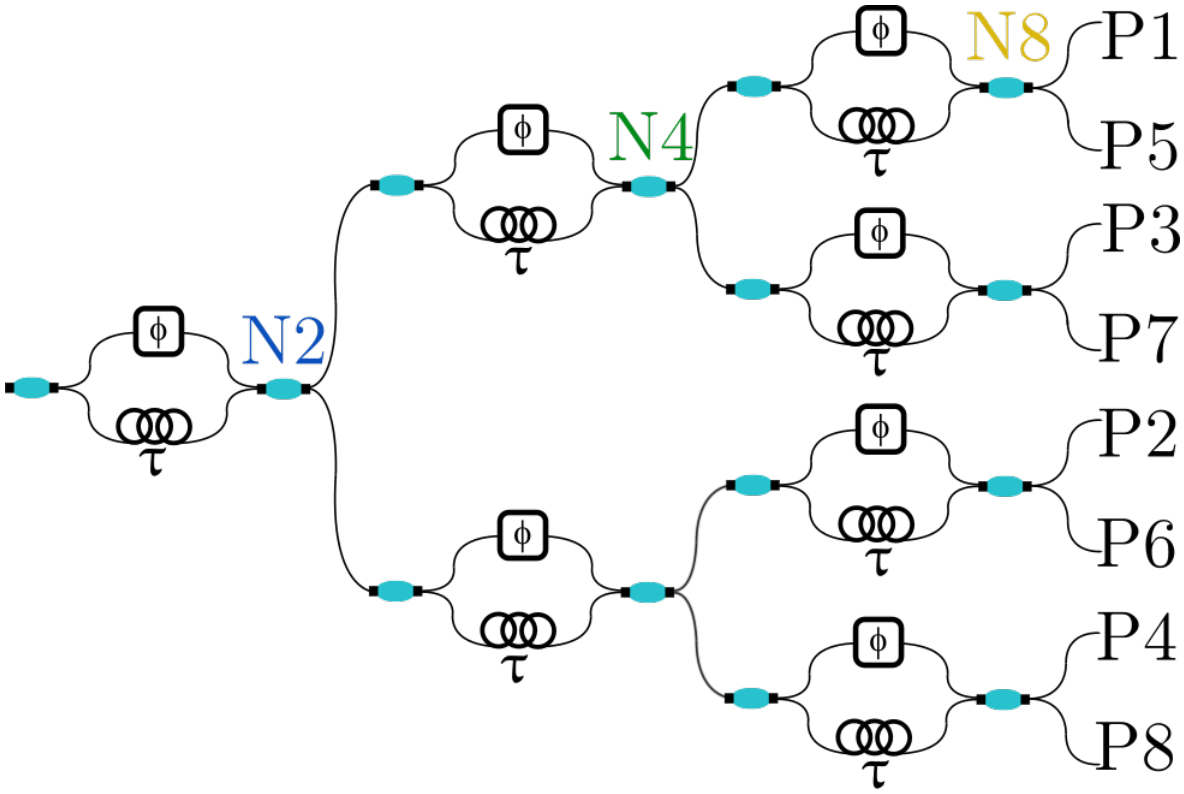

Figure 21 – Cascaded MZI to implement the optical IFFT/FFT.

This cascaded MZI setup will be further explored in details later on in this work since this device module was thoroughly developed at this research resulting in a valuable asset to our laboratory as an optical device, which can be used in other situations not exclusively at telecommunication approach.

3.2 Data modulation steps

Also from the setup from Fig. 20, the steps which transfer any data to an optical carrier are represented by three blocks the PRBS, Mapping and MZM.

The pseudo random bit source generates an aleatory sequence of bits which will represent the information to be transmitted at 12.5 gigabits per second. All this data will be sent to the Mapping block that is responsible for translating this information to electrical signals that will modulate a Mach-Zehnder. Thus, the MZM block is an array of MZMs, once each optical carrier will be modulated independently from each other, which is common to happen in a real system to better use the available bandwidth. In the cases in which different wavelengths are modulated with the same information for redundancy, as a failure strategy, the signal must travel in different paths hence as this system all carriers composed the same signal, the AO-OFDM signal, this security approach is not recommended. For this security procedure, another AO-OFDM signal should be composed with this same information.

This work selected four mapping formats to validate and be evaluated on an AO-OFDM passive optical network — two amplitude modulation formats such as on-off keying (OOK) and optical pulse amplitude modulation with four levels (PAM4). Additionally, two-phase modulation formats such as differential phase shift keying (DPSK) and differential quadrature phase shift keying (DQPSK). Those modulation formats implemented at the Mapping block are described in the following subsections.

3.2.1 Modulation Format On-off keying

On-off keying (OOK) is the most straightforward binary intensity modulation format. The OOK transmit digital data through the presence (signal ON) or absence (signal OFF) of a carrier. Therefore, OOK detection is relatively more uncomplicated when compared with other modulation formats. Moreover, OOK simplicity allows more resilience to noise on a communication system hence able to cover further distances than more complex modulation formats. Although, the OOK is not the most efficient modulation process due to its high DC value, as DC doesn't present any variation no information is transmitted also increase the power budget costs [36].

3.2.2 Optical pulse amplitude modulation with four levels

The optical PAM4 is based on the interferometric principle; two different electrical signals drive a DD-MZM hence the light recombination at the MZM output can result in four different power levels, as shown in Fig. 22a [46].

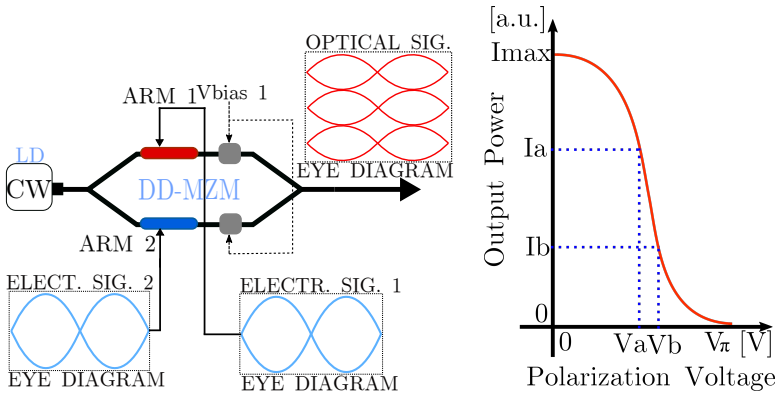

(a) Optical PAM4 implemented. (b) MZM characteristic Response.

Figure 22 – Main components to project an optical PAM4.

The optical PAM4 project is based on the intensity power output versus polarisation voltage (Vbias) response of a given MZM, as shown in Fig. 22b. Since the MZM intensity response resembles a sinusoidal curve, a conventional PAM4 is limited in the linear region between Ia and Ib hence its full modulation capacity is not used. For implementing an optical PAM4, four equally spaced power levels must be chosen such as Imax, Ia, Ib and 0 as shown in Fig. 22b. There are correspondent polarization voltages for each power level selected. Therefore, the combination of the two electrical signals with a fixed Vbias at $V_\pi/2$ should result on the found polarisation voltages. Finally, the actual values for the electrical signal can be estimated by solving the following equations [46]:

$$V_{1A} - V_{2B} - Vbias = 0, \tag{3.1}$$

$$V_{1A} - V_{2C} - Vbias = Va, \tag{3.2}$$

$$V_{1D} - V_{2B} - Vbias = Vb, \tag{3.3}$$

$$V_{1D} - V_{2C} - Vbias = V_\pi. \tag{3.4}$$

Where V_{1A} and V_{1D} are the values assumed by the first electrical signal, similarly V_{2B} and V_{2C} are the values constituents the second electrical signal.

3.2.3 Differential phase shift keying

The DPSK is another essential mapping format responsible for encoding a bit stream into phase shift variations. The DPSK key difference among other phase mapping formats is that this technique takes into account the phase variation among subsequent symbols. Other modulation formats such as bipolar phase shift keying or quadrature amplitude modulation (QAM) require a direct detection which is costly and more complex due to the synchronisation process. In contrast, as the information is stored on phase difference considering the current symbol related to the previous one, direct detection is possible when employing delay interferometers (DI), shown in Fig. 23 [36, 47].

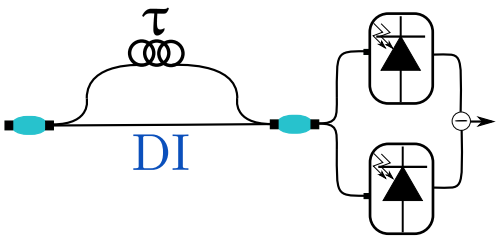

Figure 23 – Delay Interferometer.

In Fig. 23 the income signal is divided into different paths. The first path is direct to the output whereas the second path applies a time delay of a symbol period and a phase shift of zero degrees on the incoming signal. Then those two modified signals will interfere with each other at the end of the DI. Both DI output ports will wield the lights combination result although one will present the constructive interference and the other the destructive interference. In other words, both outputs will offer the same information although with opposite signs. At the receptor, just one photodetector is necessary to recover the data from either output port. However, when using two photodetectors, it is possible to increase the received signal amplitude while removing common noised among signals such as thermal noise. Also, this process can be called shelf-coherent detection [36, 47].

At transmission, the encoding process can be simply done by the eq. 3.5:

$$pk = \overline{a} * \overline{pk_1} + a * pk_1 \tag{3.5}$$

where a is the actual bit, pk is the bit to be sent and pk_1 is the previously sent bit.

3.2.4 Differential quadrature phase shift keying

The DQPSK also stores information on the phase difference of two subsequent symbols. In contrast with the DPSK, the DQPSK codify two bits into one symbol hence increasing the bit transmission rate. Similarly, the DQPSK signal can be direct detected by two DI

in parallel. Thus, the income signal is divided into two devices than further split into two paths. Both DIs will apply a time delay of one symbol period. Furthermore, one DI will also implement a phase shift of 45 degrees while the other DI will also apply a phase shift of 315 degrees, as shown in Fig. 24 [36, 47].

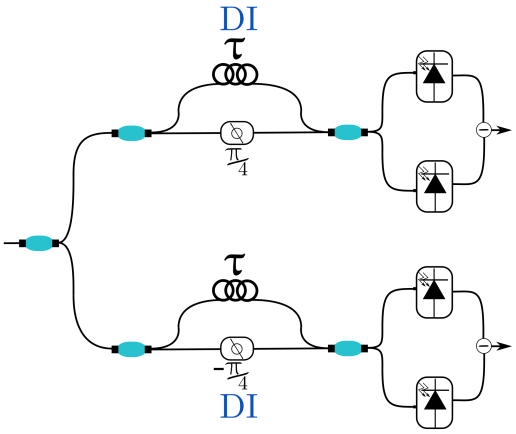

Figure 24 – Delay Interferometer.

At transmission, the encoding process can be implemented by the eq. 3.6 and eq. 3.7:

$$pk = \overline{a} * \overline{b} * \overline{pk_1} + \overline{a} * b * qk_1 + a * \overline{b} * \overline{qk_1} + a * b * pk_1 \tag{3.6}$$

$$qk = \overline{a} * \overline{b} * \overline{qk_1} + \overline{a} * b * \overline{pk_1} + a * \overline{b} * pk_1 + a * b * qk_1 \tag{3.7}$$

Where a and b are the actual bits to be converted, pk and qk are the bits to be sent, pk_1 and qk_1 are the previous bits sent. Furthermore, analysing the pk_1 and qk_1 truth table sobreposition 1 sheds a light on the process realized by equations 3.6 and 3.7.

Table 1 – DQPSK encodding pk and qk truth table sobreposition.

		Actual Bits			
Past Bits		**00**	**01**	**11**	**10**
	00	11 0°	01 90°	00 180°	10 270°
	01	10 270°	11 0°	01 90°	00 180°
	11	00 180°	10 270°	11 0°	01 90°
	10	01 90°	00 180°	10 270°	11 0°

Table 1 is constructed based on the actual bits to be transmitted (ab) and the past bits transmitted (pk_1qk_1). As a result of ab and pk_1qk_1 combination is possible to find the

next bit to be transmitted represented in blue, which is equivalent to a phase variation represented in red. Finally, it is important to mention that at the receptor no decoding is needed as the parallel DIs convert the optical signal to the electrical domain while automatic decoding the transmitted information [36, 47].

Equation 3.6 can be found by solving the Karnaugh map taking just the first bits in blue. Similarly, eq. 3.7 can be found by solving the Karnaugh map taking only the second bits in blue.

3.3 Component blocks

The other blocks displayed in PON setup already mentioned are implemented in a more straightforward fashion such as the RX and TX blocks, or they will be lattely describe since they represent a significant result from this work as is the case of the OFC block.

The TX block here used is shown just at the optical network unity side because it represents a more complex system earlier mentioned in this text. The Mapping and MZM blocks compose the TX block, once its aim is to imprint the user data into the upward optical carrier sent by the OLT and selected by the OFFT block.

The RX block is also a generic component, and it represents the photodetector primarily. In the case when phase modulation is used at the RX block will also include the interferometric process which converts phase variation into amplitude variation by passing the incoming signal through a DI.

The ODN block for this simulation works only as a power divider, and in other words, the signal is equally split to all ONUs. This block does not affect the system behaviour once thermal noise or dark noises are not in focus on this study. Thermal noises, non-linearities and dark noises represent a significant impact at the reception of the signal, once they mainly compose the ground noise floor of the system. Since this research evaluated the effects of cross talk noise and possible mitigations, power splitters will not affect the result because the signal and the noise will be under the same division, in other words, the noise floor and the signal will be at the same distance even after a power splitter.

3.4 Simulation Structure

In this section is describe two main program flows that composed the whole system simulated. The first set of charts represent the flow of the main program, which is the telecommunication system with its components. The second set of diagrams describe the process to generate the OFC.

3.4.1 Flow chart of the data transmission System

The logic of the telecommunication system here simulated is shown on the Fig. 25. The main goal is to initialise the previously construct OFC and select the nature of the signals to be transmitted, preferably optical or electrical. Then the signal is modulated accordingly, and the AO-OFDM symbol is created and assembled with the downstream carriers. At the reception, all information is recovered, and new data is stored at the upstream channels. Thus, the AO-OFDM symbol is created and send back to the OLT in which the data will be recovered.

Within this core code, there are blocks written "Start". Those boxes represent new function blocks that are called to give the code sequence as they have specific functions.

The "Start Data Down Stream Optical Transmission" is shown in Fig. 26. This diagram displays the main parts to generate the data to be transmitted and its transmission. Firstly, the OFC is split into individual carriers then data is randomly, and the electrical modulating signal is created with them. Thus, the modulating signal stores the information into optical channels. Before, sending the data, the optical signal is assembled to form the AO-OFDM symbol that will be transmitted through a path. The "Start Data Up-Stream Optical Transmission" shown in Fig. 27 it has similar behaviour with its previously described chart the only difference is that here the optical carriers will always be separated by the AO-FFT function the previous code it also could be done by a set of ideal-Gaussian-narrow filters.

The "Start Data Down Stream Optical Reception" and the "Start Data Up Stream Optical Reception", shown in Fig. 28 and Fig. 29 respectively, present the same logical flow. The incoming AO-OFDM symbol is separated by the AO-FFT function. Therefore, the data is recovered accordingly with the modulation format. Then, the BER is measured, and its value is stored for future evaluation.

The "Start AO-IFFT" shown in Fig. 30 is responsible for orthogonally assembling all optical carriers. It applies the current time and phase delay on the first two incoming optical fields. Then, it verifies whether the process reached an end. If not, the next time and phase delays are calculated, and this same function is called for applying this process on the upcoming odd carrier in line. Then this function is called again for implementing this process on the next even carrier in line. The results from odd and even calculations are stored, and the program returns to where it was called. If yes, the results are stored, and the program also returns to its last call. The "Start AO-FFT" represented in Fig. 31 is similar. The only difference is that time, and phase delays are applied to split the carriers instead of assembling them.

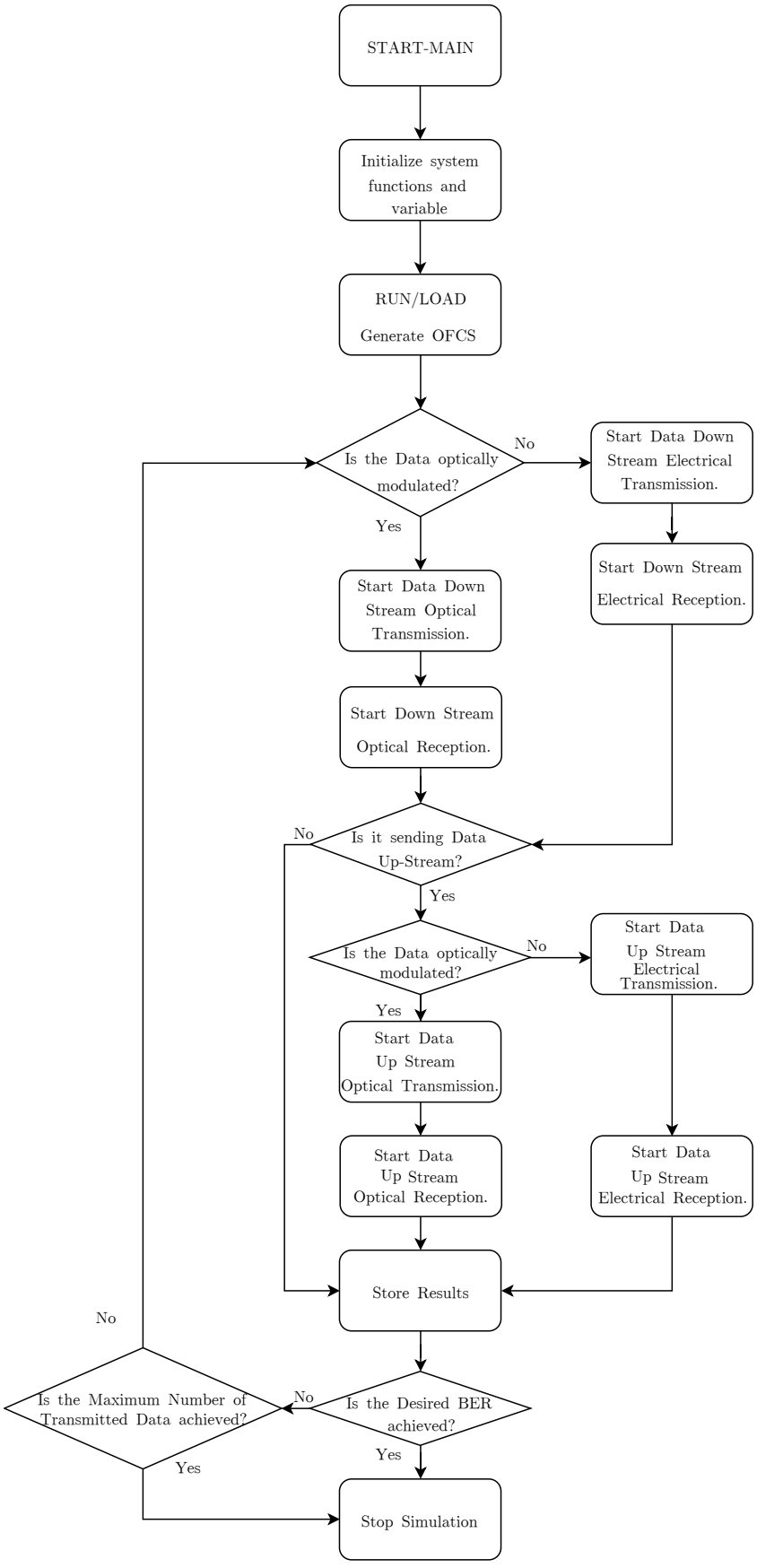

Figure 25 – Flow Chart of the Simulated Main Code.

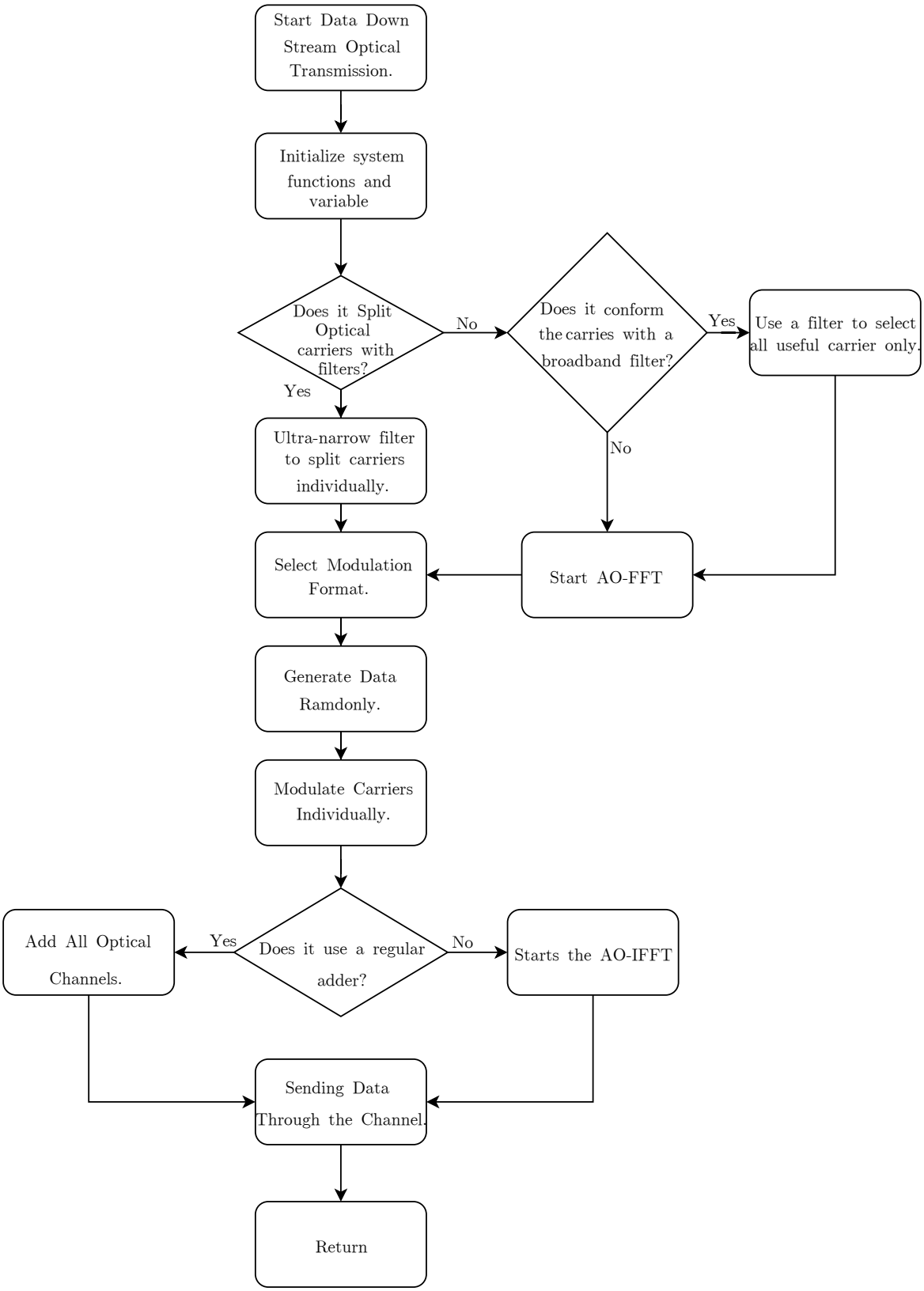

Figure 26 – Flow Chart of the down-stream transmission simulated code.

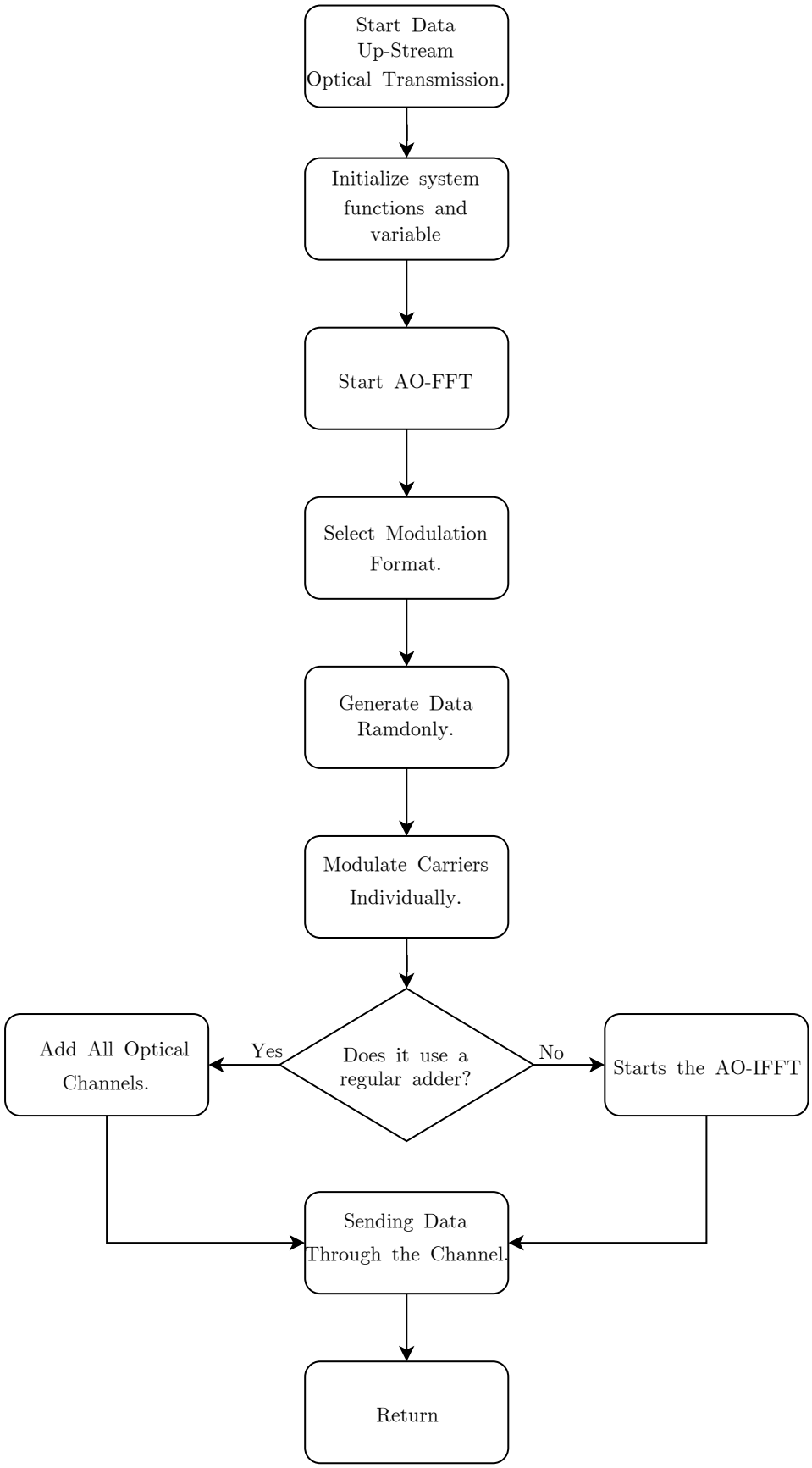

Figure 27 – Flow Chart of the up-stream transmission simulated code.

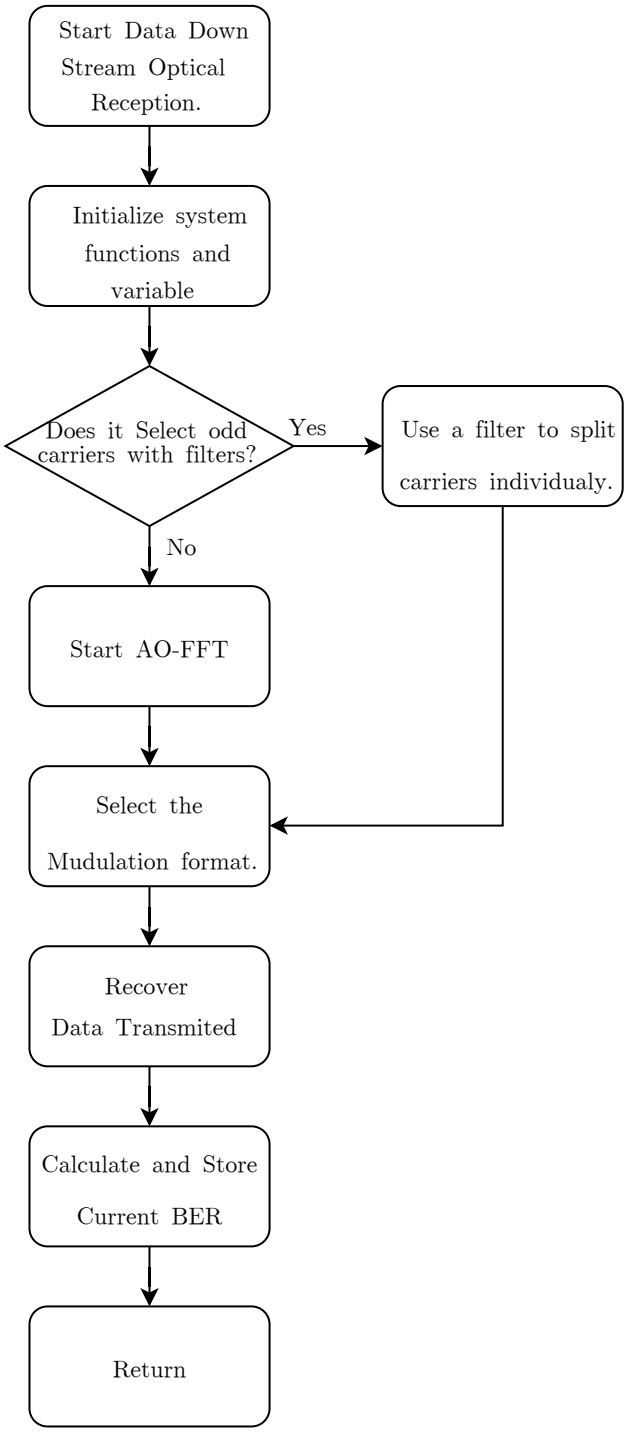

Figure 28 – Flow Chart of the down-stream reception simulated code.

3.4.2 Flow chart of the OFC generation

The generation of OFC was the first step created once. All the signals will depend on the quality of the optical channels. The "Start Generate OFCS" shown in Fig. 32 display the main points of the system used to create all the optical carriers. The file with MZM is loaded, and the electrical signal that will modulate the incoming CW is created. Then the optical ring is called. On the return of the function, the recent created OFC is measured,

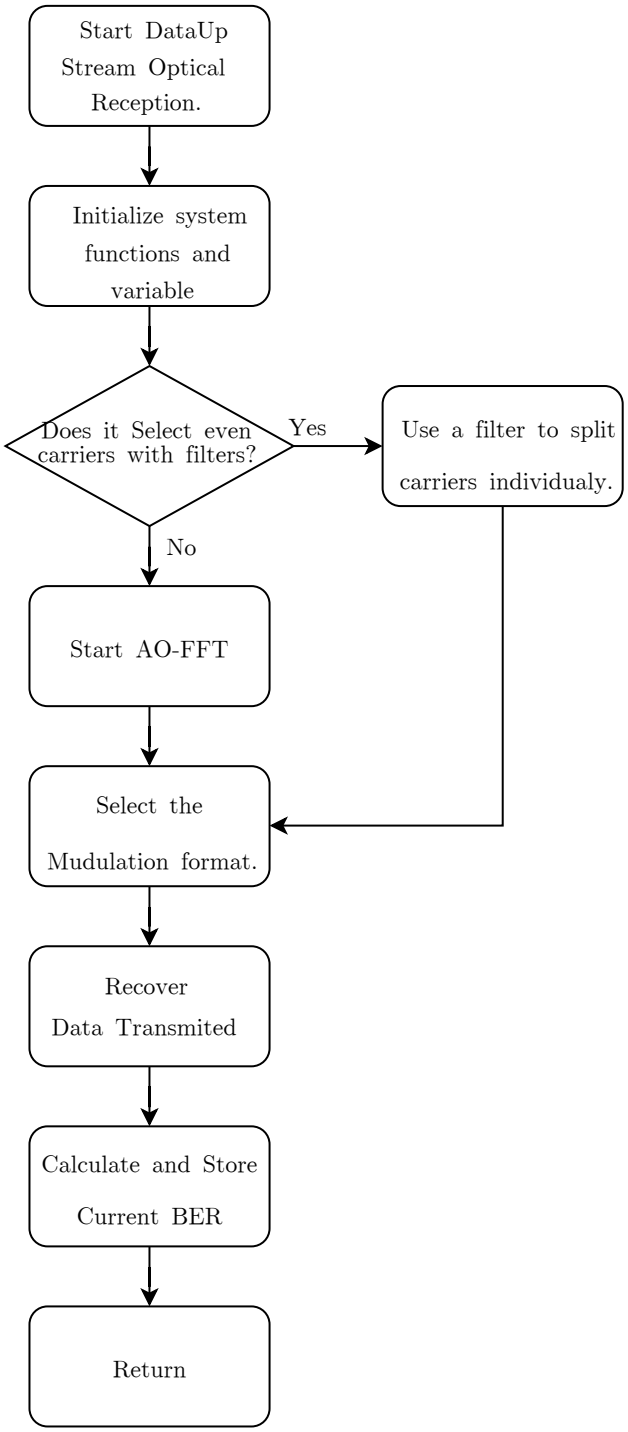

Figure 29 – Flow Chart of the up-stream reception simulated code.

and the main data is stored for future usage.

The "Start Optical Ring" shown in Fig. 33 is the main points implemented to create the optical loop. With the initialised input and output fields the program introduces the CW source and verify if it already achieved the maximum number of interactions. If not, the optical field is modulated, filtered amplified and sent back to the beginning of this loop. If yes, the OFC is read, and this function returns at its last call.

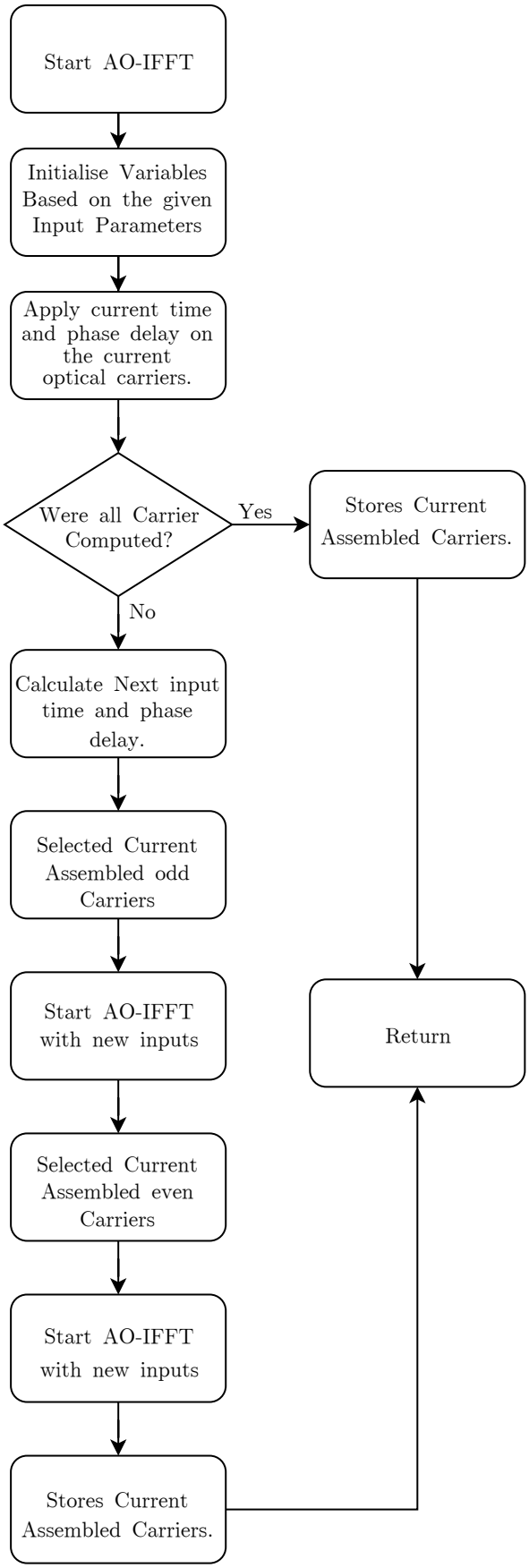

Figure 30 – Flow Chart of the all-optical inverse fast Fourier Transform simulated code.

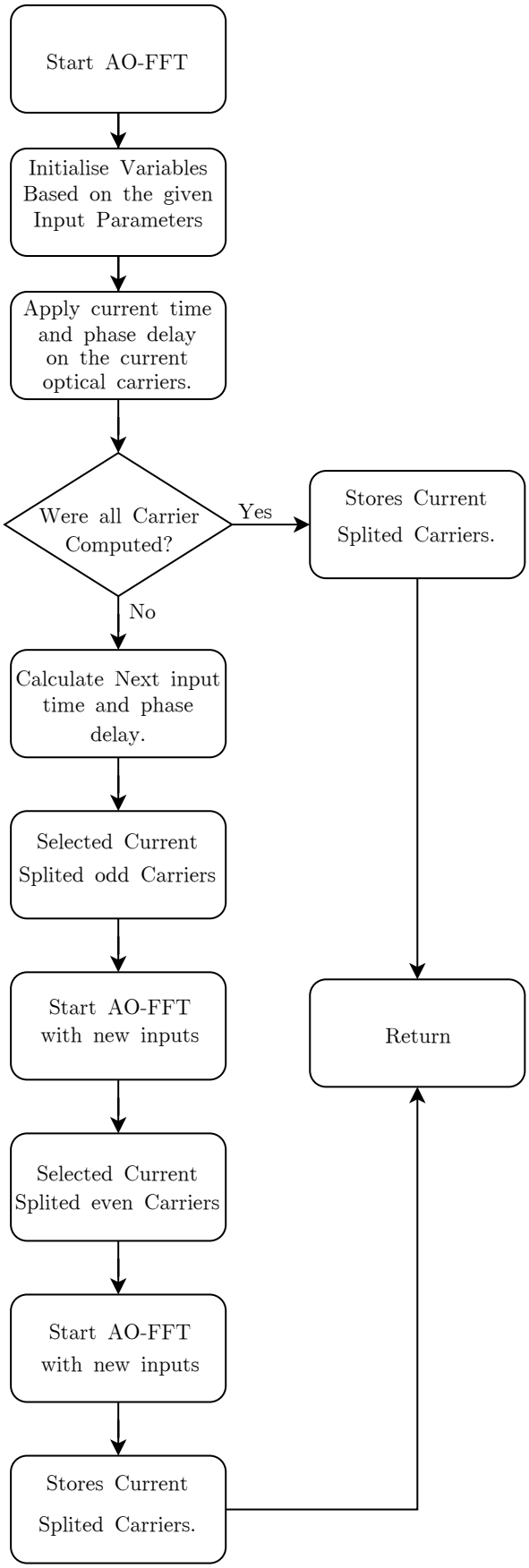

Figure 31 – Flow Chart of the all-optical fast Fourier Transform simulated code.

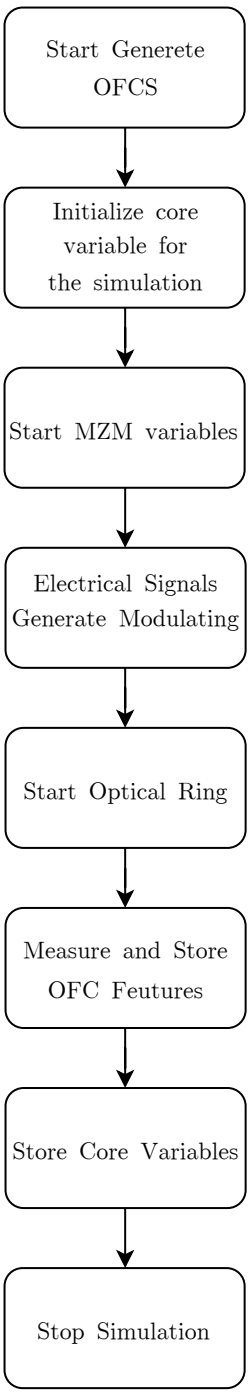

Figure 32 – Flow Chart of the optical flat comb generation code.

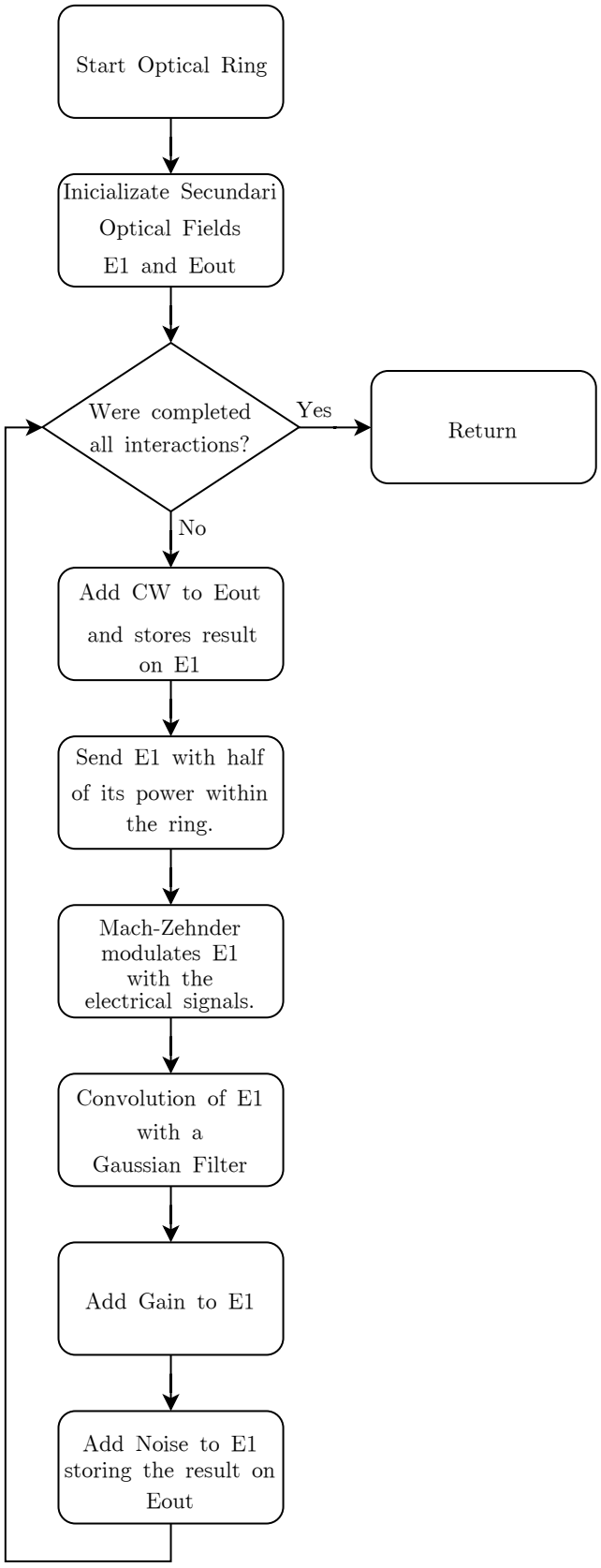

Figure 33 – Flow Chart of the RFS process on the optical ring code.

4 Results and conclusions

After defining the system to be evaluated, it was necessary first to verify whether the system behaves like a real experiment. It is essential to highlight that all results here shown were achieved from simulations, when not stated otherwise, based on models constructed on the simulation environment. Therefore, the first results achieved at this work are respective to validate whether the components and systems implemented are compatible with representing a real case of study. Thus, it is essential to highlight that a figure of merit used at this work was based on the bit error rate (BER) over SNR. This BER over SNR comparison aims to verify how close theoretical and the simulated responses are close together, which the ideal is to make the simulated results as close as possible to the ideal curves. Moreover, this chapter presents the results obtained from the study done on our PON setup architecture as well as on specific components. As a result, the end of this chapter aims to highlight the advantages on using the devices presented in this work as well as to give an overview of the benefits they will bring for future passive optical networks, which will be highly demanded in the future as predicted.

Apart from the MZM characterisation results, all the following results here presented were simulated. In other words, despite the MZM validation, all others validation and evaluation results were achieved through simulation on software such as MatLab. The algorithm used on those results was shown in the previous chapter, from which the vast majority of result here presented were extracted. Moreover, the theoretical curves here mentioned were created on MATLAB, which uses the model of a single channel back-to-back transmission on the baseband

4.1 Mach-Zehnder modulator model

The first model validated was the Mach-Zehnder modulator due to its importance for this work. For instance, all modulation formats here used were based on a DD-MZM model as shown in eq. 2.14. The only exception was the DQPSK implemented by an IQ-MZM. The MZM equation was adapted and then compared with the response of an actual IQ-MZM device, the LN86S-FC, as shown in Fig. 34. For this experiment, a tunable laser was used, connected by computer with the network card TXP 5016 from Thorlabs the laser card LS5 TXP centred in 1550,12 nm was used at 1550 nm as CW mode with 0 dBm of output power. The MZM was powered by the DC power source 2231A-30-3 from KEITHEY. The MZM output was measured by the power meter FPM-300 from EXFO and values noted in a table. For this experiments the voltage values started at -8 volts and was change 0.2 by 0.2 volts until 8 volts aiming to evaluate the MZM characteristic curve.

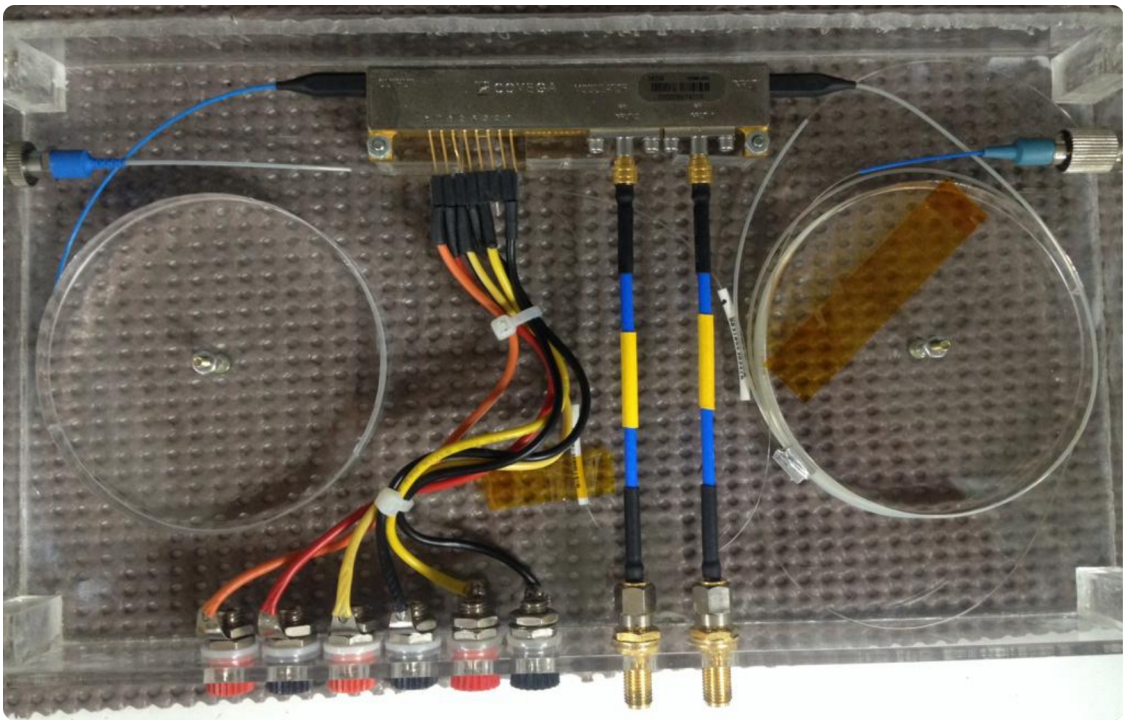

Figure 34 – Mach-Zehnder Modulator LN86S-FC.

Fig. 35 compares the simulated IQ-MZM with the actual device. The markers represent the data collected from laboratory whereas the continuous lines represent the simulated results. The IQ-MZM has three distinct polarisation voltages. Therefore, in Fig. 35 each colour represents one polarization voltage variation. While varying the bias voltage, the other two terminals were connected to the ground.

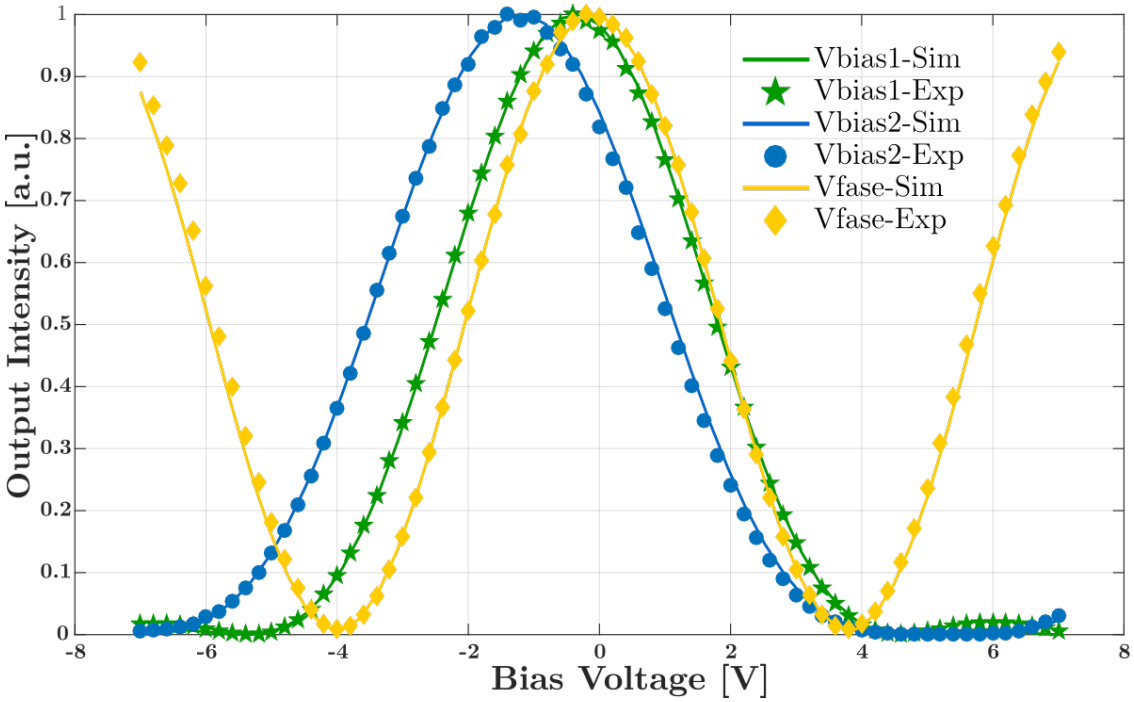

Figure 35 – IQ-MZM characteristc curve.

The adjustment done was related to the MZM characteristic voltage (V_π). For the blue curve, V_π was set to be 3.1 V whereas for the green curve V_π was set to be 3.25 V. The yellow curve, representing the phase variation, an offset voltage of 1.85 V was needed.

4.2 Optical flat comb achieved

The optical flat comb source is represented in Fig. 36. Besides, the CW at 1550 nm, was considered to be at zero Hertz highlighting the spacing among carriers. A closer look at optical carriers power peak fluctuation is displayed on the depicted figure with a maximum amplitude of difference 0.3 dB in the OFC spectrum.

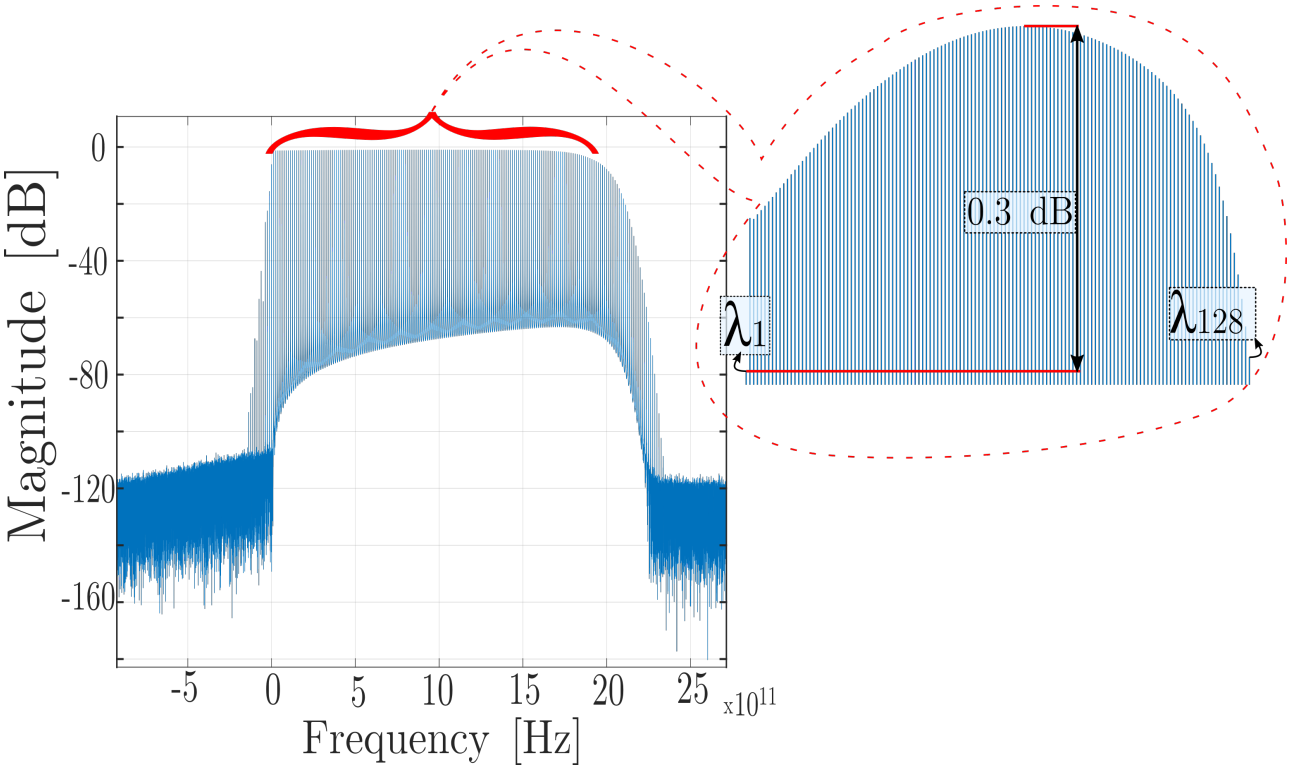

Figure 36 – Optical flat comb source generated by recirculation frequency shifting process.

Once the MZM model was obtained, the generation of multiple wavelengths were the first results that we aimed to achieve. Thus, among different methodologies, this work selected the RFS technique, which can generate numerous carriers from a single CW source by shifting the incoming light at each round trip on the optical ring. Thus, this work considers the CW at 1550 nm with one polarisation format. The DD-MZM had been configured with characteristic voltage (V_π) of 3.8 V setting the modulator polarisation voltage (Vbias) as $V_\pi/2$. The BPF had been configured with 32 nm of bandwidth. The OA had been configured with 3.2 dB of optical gain and 20 dB of saturation gain. Also, the RF signal driving the DD-MZM had been generated with one sinusoidal tone of 12.5 GHz hence achieving approximately 0.1 nm spacing among carriers. Furthermore, over three hundred carriers were created although for a 0.3 dB of flatness only 128 equally spaced channels had been selected.

The main reason for choosing this OFC setup as spacing among carriers was its flexibility to tune spacing among carriers by an RF signal. As a result, carriers spaced by transmission symbol rate had been achieved. Although, devices frequency response limits the spacing

tunning process. Hence, finding devices such as MZM with an operational range over 50 GHz can be challenging also more susceptible to dispersion, as previously mentioned 1.4. At this work, multiple carriers were used to increase system throughput without significantly increase symbol rate hence minimising dispersion.

4.3 OIFFT effect at transmission

This work second step was to achieve an optical device able to split the various optical carriers previously generated precisely. However, this device must have some characteristics such as to preserve the carriers orthogonality, ready to make the reverse process, which means assembling different wavelengths, also avoiding interference among adjacent channels. Those characteristics are present on the Fourier transforms as previously mentioned also it was seen the possibility of implementing it on the optical domain. Therefore, an algorithm was implemented mostly based on the optical coupler equation 2.15 adding just a time and phase delay where those were needed. As a result, this research performed a device able to reproduce the FFT and the IFFT at the optical domain of N points, where N is the number of points of the FFT/IFFT. This algorithm recursively allocates MZI, based on optical couplers, and automatically calculates the correct time and phase offset needed to implement at the optical domain an FFT or IFFT of N points. Furthermore, as this algorithm was implemented as general as possible, it can be applied in different areas, such as distributed sensors, integrated optics, clock references. Thus, this device model is also an essential contribution to the laboratory where this research was developed.

Furthermore, the crosstalk noise in the passive optical network is a well-known issue and has a significant impact on system performance [48, 49]. Recent researches [50, 51, 52] have been presenting new approaches to mitigate this issue. Differently from those cited works an architecture based on AO-OFDM has the advantage of reducing crosstalk noise at optical channels combination process, which is critical for the upstream transmission.

By taking the cascaded MZI impulse response, as shown in Fig. 37, it is possible to observe its output frequency response, which is a set of orthogonally spaced, tunable filters. Thus, from left to right, the OFFT process can be understood as an income optical OFDM signal that has its carriers selected by a filter. Each MZI output port (Pn - n vary from 1 to the FFT points number) will be tuned for one OFDM optical channel. The filter bandwidth and frequency need to be adjusted accordingly with the OFDM signal by adequately setting the phase and time delay in each MZI. Thus, this set up can be tunable to a different system by just altering those parameters.

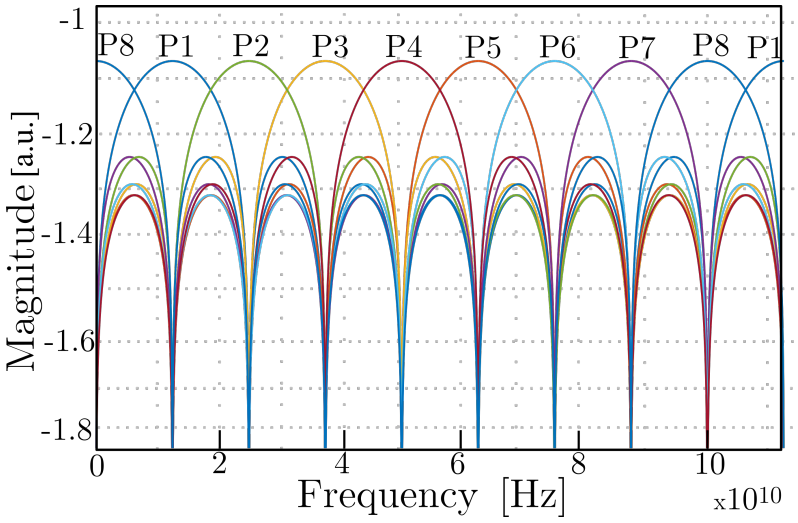

Figure 37 – Cascaded MZI impulse response.

To better understand the relevance of this setup a closer look to the interferences mitigated in one optical channel was taken as an example. The optical IFFT implemented preserves carriers orthogonality and also avoids approximately 20 dB of crosstalk noise when compared with a conventional combiner. Figure 38 shows the leaking of the crosstalk noise within an optical channel comparing two different scenarios A and B.

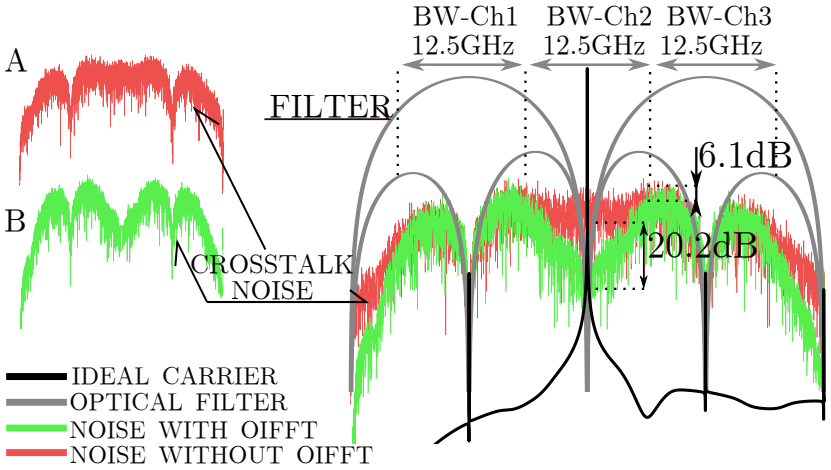

Figure 38 – Comparison of noise effect on upstream carrier in different setups.

The curves are acquired after the OFFT process in a downstream transmission. The ideal carrier, without any noise or modulation, is located at channel two (Ch2). Ideally, any noise from adjacent channels should be present at Ch2. However, when a conventional combiner was used, instead of the OIFFT, to assemble the all-optical OFDM signal crosstalk noise was detected in the Ch2 at receiver, represented by the A setup. The OIFFT implemented can be seen as an optical filter responsible to attenuate all frequencies outside its bandwidth. The B setup implements the OIFFT and the filter response on adjacent carriers is shown in Fig. 38. Although the OIFFT was implemented, Ch2 presented noise at the receptor. In contrast, the noise on B setup was significantly less than the noise presented at A setup, achieving less than 20 dB at the carrier frequency. Thus, the explanation for the gain in signal clarity is the behaviour of the OIFFT as it acts as an orthogonal tunable filter and as shown by [34] when the OIFFT/OFFT pair has used the orthogonality of the signal is preserved which ensures the signal recovery capability.

4.4 System performance evaluation for different modulation formats

At this point, the all-optical OFDM signal was compared with a theoretical response. Even though the theoretical curve is for single carrier transmission system whereas an OFDM signal works multiple tons, this validation is still correct because an OFDM system must present the same performance as a single carrier system. Therefore, this procedure aims to analyse the bit error rate (BER) against the noise density per bit (EbN0). Thus, the AO-OFDM, with 128 optical carriers, was sent in simple back-to-back transmission and at the receptor, white Gaussian noise was added. The forward error correction (FEC) of 7% ($3.8\text{x}10^{-3}$) was set as a performance threshold as recommended for optical communications [53]. This variable is used as a portion of data stored on the payload with a know bit sequence that will be used on the error correction algorithm. The size of this known information can vary depending on your application. However, the less space this data occupies, the better once more free space will be available to transmit information. Thus, with an FEC filling, 7% of the information payload is equivalent to set a BER of $3.8\text{x}10^{-3}$.

Fig. 39 shows the block diagram of the generation process of the electrical signal, which will drive the Mach-Zehnder. For all modulation formats, a pseudo-random bit source (PRBS) will generate the data to be transmitted. Therefore, the bits will be assembled in groups accordingly with the modulation process hence, each group will be encoded into symbols. Then, the generated symbol will be converted to the analogue domain. Finally, before arriving at the MZM, the signal will be divided into two paths that will also add a phase shift among signals accordingly with the modulation format.

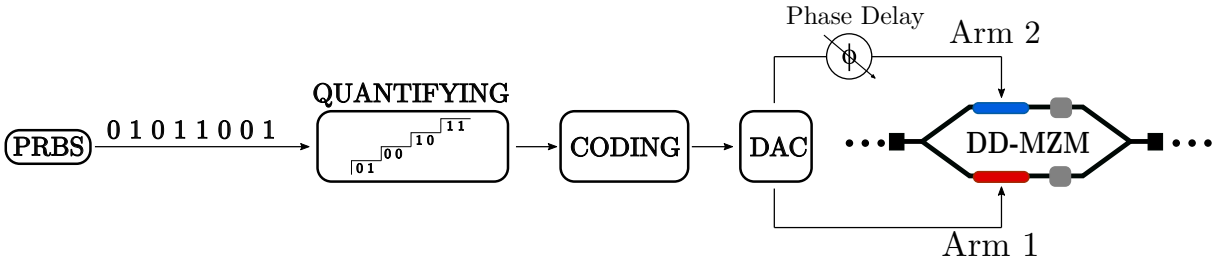

Figure 39 – Block diagram of MZM driven signal generation.

For the OOK and the DPSK, a DD-MZM is used to print the signal information into the laser beam and both has a phase delay of π radians hence implementing a push-pull configuration for the module. However, the optical PAM4 also used a DD-MZM each arm of the modulator will receive a different electrical signal thus, push-pull configuration ideal to minimise chirp noise is not possible. In contrast, the DQPSK modulator uses an intensity quadrature Mach-Zehnder modulator (IQ-MZM) and similarly to the optical PAM4 each modulator arm will receive a different electrical signal.

4.4.1 Modulation format: On-off keying

The comparison between the OOK theoretical response and the simulation response is shown in Fig. 40. The theoretical curve, represented in black, was calculated by the mathematical program for a given EbN0 input value. The simulated curve, represented by orange diamond markers, is from the AO-OFDM signal where just one optical channel is used. The simulated curve, represented by blue markers, is the result when all optical channels were used. Here, 128 optical carriers were individually modulated by an OOK process implemented by a DD-MZM. The electrical signal driving the optical modulator is a rectangular pulse due to digital to analogue conversion from a pseudo-random bit source (PRBS). The electrical signal had an amplitude variation from 0 V to 0.95 V, and it is incoming on the first arm of the DD-MZM. A copy of this signal with a phase shift of 180 degrees is applied on the modulator second arm. Besides allowing an amplitude swing of 1.9 V, this configuration is necessary to minimise chirp noise [54]. The Mach-Zehnder had a V_π of 3.8 V hence polarising it on 1.9 V.

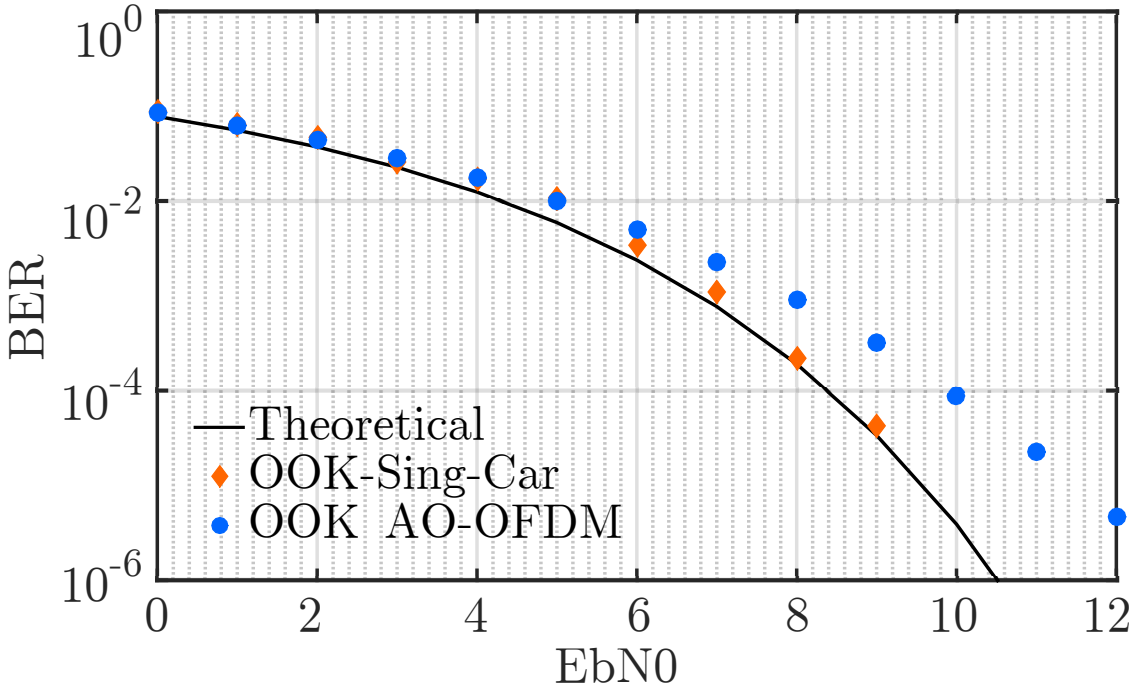

Figure 40 – OOK bit error rate against energy bit per noise density.

4.4.2 Modulation Format: Pulse amplitude modulation 4-level

For this analysis, it was considered a DD-MZM with a V_π of 3.8 V and polarised on 1.9 V. For the PAM4 electrically implemented the signal amplitude vary from 0 V to 1 V to keep the signal on the modulator's linear region. The unipolar signal was selected because the MZM was configured to work as a push-pull setup. Therefore, the second signal, which is a copy from the first one, has an amplitude variation from 0 V to -1 V.

In Fig. 41 the optical PAM4 was compared with its theoretical curve, and besides, it was also confronted with a PAM4 electrically implemented. As previously mentioned, the theoretical curve is represented in black more over the applied signal with only one carrier is depicted in orange by diamond markers and in green by star markers, respectively for PAM4 optically and electricity implemented. At first glance, there is a difference from the theoretical response to the simulated result of almost 3 dB when just one carrier was used. Now, when evaluating the AO-OFDM signal, the difference is expressive. The BER response with all 128 carriers combined is represented in blue by circular markers for the PAM4 optically implemented, in contrast with the electrical PAM4 which is depicted in dark-blue by star markers.

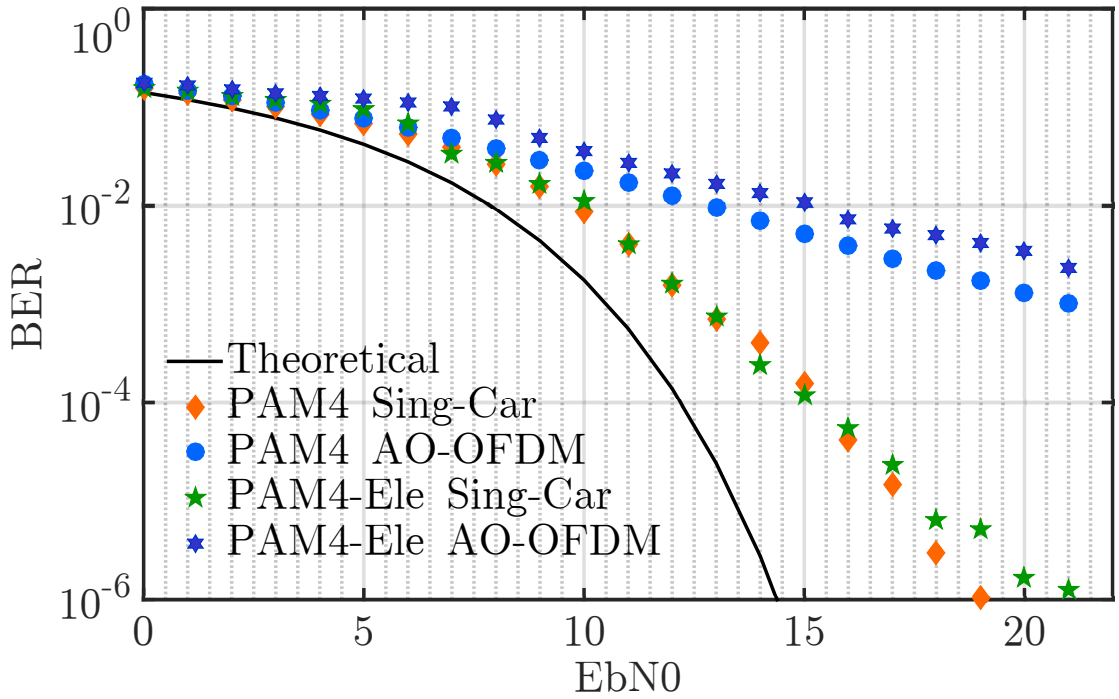

Figure 41 – PAM4 bit error rate against energy bit per noise density.

From this first analysis, it is possible to see that the optically implemented Fourier transforms impact significantly the PAM4 modulation format. Although the single carrier result is far away from what is expected, the AO-OFDM should present a close behaviour to the single carrier curve however as their distance of almost 9 dB it represents a significant toll to be paid for the AO-OFDM to be implemented with either the optical or the electrical PAM4 modulation.

The penalty presented in Fig. 41 is due to the amplitude distortion caused by the MZI. The amplitude modification becomes more evident when we analyze signals eye diagrams in two cases one with a signal passing through the MZI set up and another one with the

signal passing through a regular filter as shown in Fig. 42. Noticing the top eye diagrams refer to the optical PAM4 while the bottom diagrams represent the electrical PAM4. The figures on the left represent a signal without the OIFFT/OFFT implementation while the right figures represent the signal with OIFFT/OFFT set up. It is possible to see from Fig. 42a and 42c the effect on inter-carrier interference (ICI) as no other source of noise was considered on this back-to-back communication test. The interference was significantly reduced when the MZIs were used as shown in Fig. 42b and 42d. However, the distortion caused by the MZIs affected more the electrical PAM4 in Fig. 42d as the eye-opening are more narrow than the PAM4 optical implemented in Fig. 42b. This degradation in performance of the electrical PAM4 was the main reason to select the optical PAM4 modulation format.

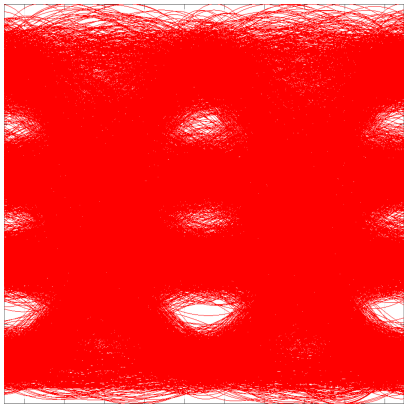

(a) Optical PAM4 with ideal filters.

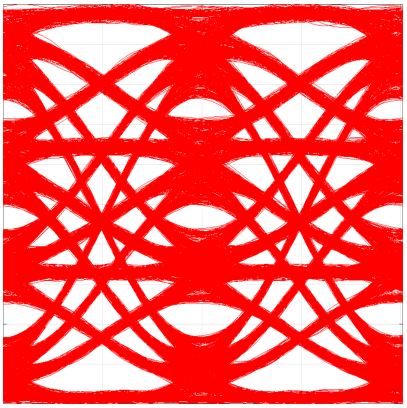

(b) Optical PAM4 with OIFFT/OFFT.

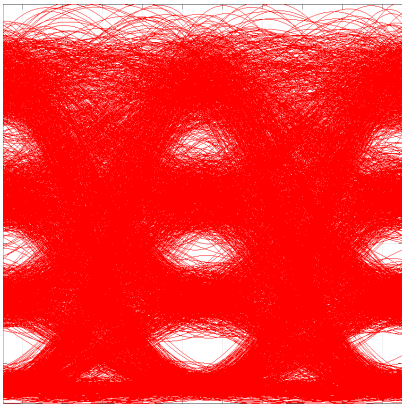

(c) Electrical PAM4 with ideal filters.

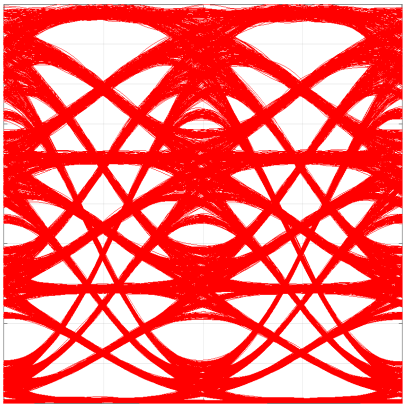

(d) Electrical PAM4 with OIFFT/OFFT.

Figure 42 – Comparing eye diagrams of a PAM4 optically and electrically implemented transmitting an AO-OFDM signal with 128 optical carriers. On here the result is observed on the 125th carrier. a) shows an optical implementation without an OIFFT/OFFT setup, instead an simulated ideal filters where used to split the channels. b) shows the same simulation as a) when OIFFT/OFFT was used. c) shows an electrical implementation without an OIFFT/OFFT setup, instead an simulated ideal filters where used to split the channels. d) display the same simulation as c) when the OIFFT/OFFT setup was used.

4.4.3 Modulation format: Differential phase shift keying

Validation of the DPSK modulation format is shown in Fig. 43. Here again, the main aim is to observe how close the simulated results are to the theoretical curve, which is represented in black. When a single carrier is sent into this system, its response, that is represented by orange diamond markers, displays the same trend although with less than 1 dB of offset to the origin. Moreover, observing the combined response of all carriers on the AO-OFDM signal, which is shown by blue circular markers, it is seen that both responses (single carrier and multi-carriers) have a close correspondence. The only difference is that the AO-OFDM signal was degraded by less than 1 dB. Thus, it is valid to expect that the DPSK results will be accordingly with what is expected on actual systems.

For those simulations, a DD-MZM with V_π of 3.8 V was also used polarised on 1.9 V. The modulator was set to work in Push-Pull configuration hence the electrical signal amplitude was limited to vary from -0.95 V to 0.95 V.

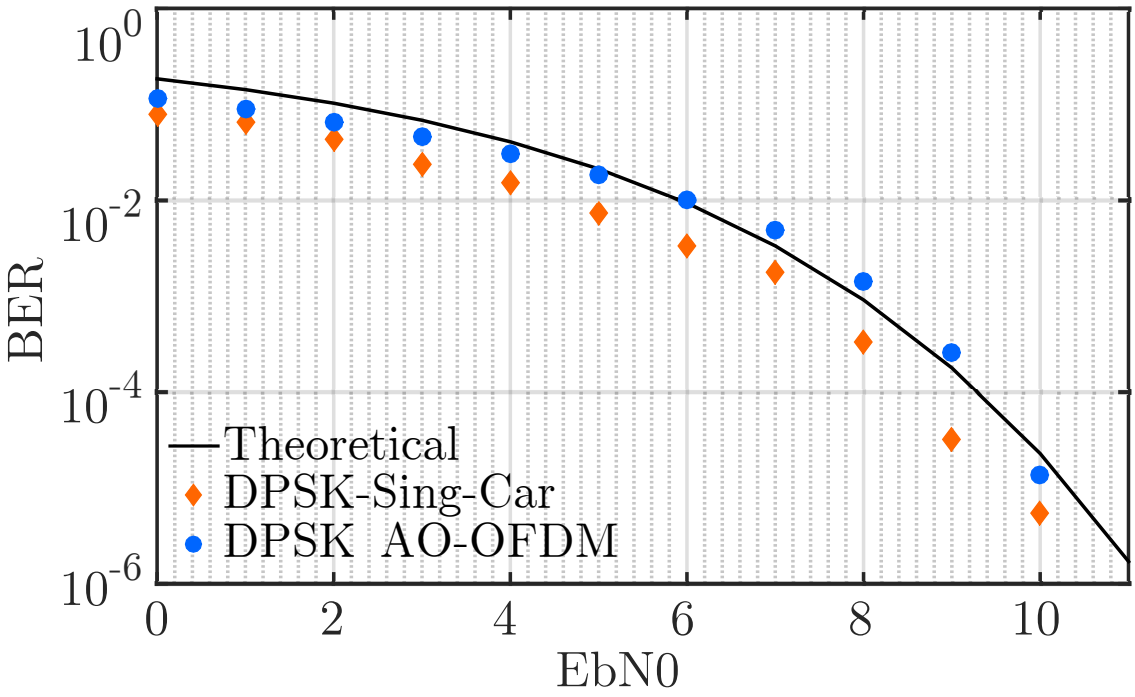

Figure 43 – DPSK bit error rate against energy bit per noise density.

4.4.4 Modulation format: Differential quadrature phase shift keying

The results obtained from the DQPSK validation are shown in Fig. 44. Likewise, the theoretical curve is represented in black while orange markers represented the single carrier signal. Besides, full circles in blue colour represented the signal with multiple carriers. A single carrier signal had similar behaviour as observed to the theoretical curve with degradation of 1 dB hence within an acceptable range. Likewise, when the AO-OFDM signal was evaluated there was a toll of 1dB compared with a single carrier signal as a result of the amplitude distortion caused by the MZIs set as the DQPSK stores information not just in the signal phase and also its amplitude. For this simulation, an intensity quadrature MZM (IQ-MZM) was used. This work considered the IQ-MZM as a low chirp device and with a fixed phase offset among each arm of ninety degrees. This work assumed a V_π of 3.8 volts, meaning that each arm was polarised with 1.9 volts. Meanwhile, the signal amplitude was limited from -0.95 V to 0.95 V.

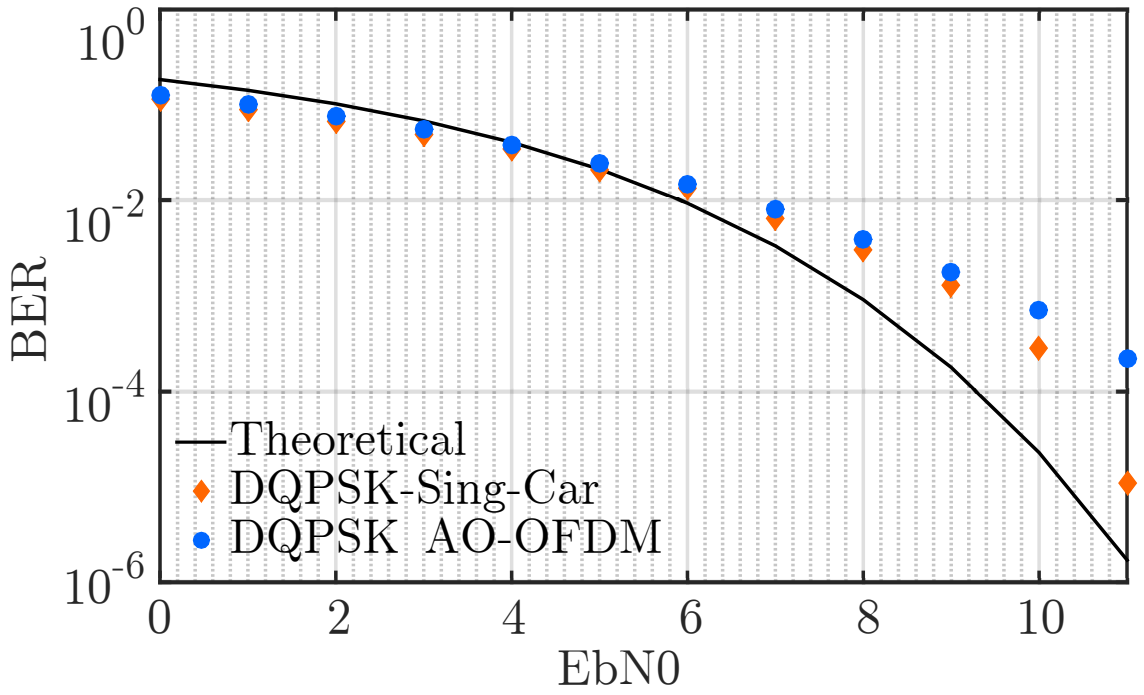

Figure 44 – DQPSK bit error rate against energy bit per noise density.

4.5 Proposed architecture evaluation

This section evaluates the proposed architecture performance due to chromatic dispersion over a standard single mode fibre (SSMF). Moreover, understand how to measure the system capacity is an essential point for bearing on the mind. Thus, knowing that each optical channel occupies a bandwidth of 12.5 GHz hence the maximum symbol transmission capacity is 12.5 GSamp/s. Therefore, if the modulation used stores one bit per symbol, one optical channel will be able to transmit 12.5 Gbps. If the modulation format stores two bits per symbol, one carrier can deliver 25 Gbps. Taking into account the need for redundancy of the signal to be transmitted 10 per cent of the available bandwidth will be used for redundancy, giving us a maximum capacity of 10 GSamp/s. Thus, when 128 carriers are divided to cover the upstream and downstream demand, the full system will have a symmetric capacity of 640 GSamp/s. In other words, the system will able to transmit 1.28 Tbps when a two-bit per symbol modulation format is used.

On this step, each modulation format is used for composing an all-optical OFDM signal with 128 channels where each channel transported $3.072 \text{x} 10^6$ bits. Differently from the previous section, now the proposed architecture BER against distance response is compared with another architecture without the optical IFFT. Furthermore, in Fig. 45, DPSK modulation is represented by diamond markers, while DQPSK is presented by circle markers. Also, in Fig. 45, AO-OFDM architecture is described in blue while the architecture without the OIFFT is depicted in orange.

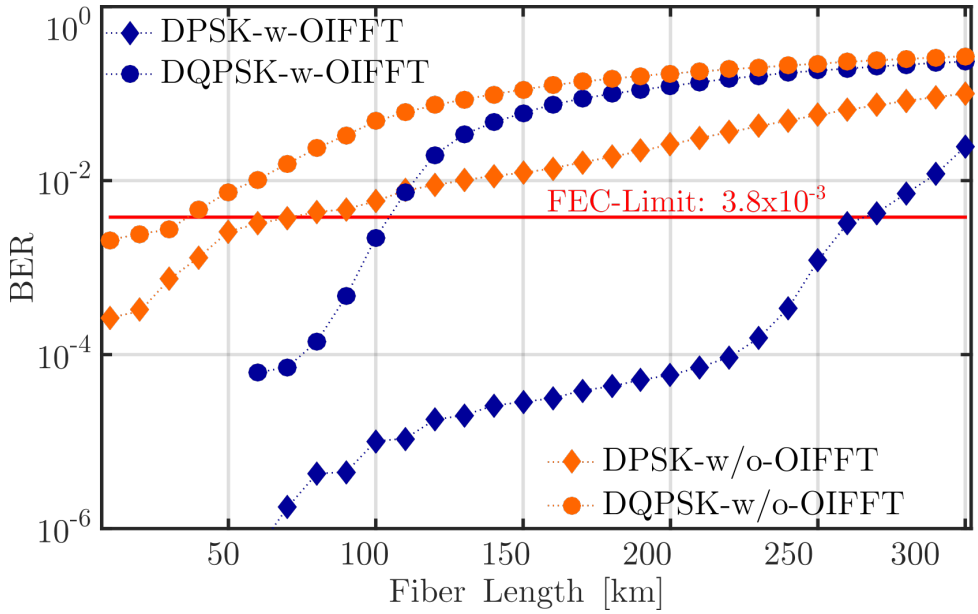

Figure 45 – DPSK and DQPSK evaluation.

Likewise, in Fig. 46, the OOK modulation is displayed with diamond markers while the PAM4 is represented by circle markers. Besides, in Fig. 46, this paper proposed architecture is depicted in blue while the system without the OIFFT is represented in orange. The AO-OFDM had a better performance over distance than an architecture without the OIFFT, as shown in Fig. 46 and Fig. 45. The optical IFFT prevents approximately 20 dB of crosstalk noise, hence it was expected a performance degradation due to SSMF features. The performance degradation is compared considering 70 km of SSMF as shown in Fig. 46 for OOK format with the OIFFT compared with the OOK without the OIFFT. The PAM4 with the OIFFT, when compared with the PAM4 without the OIFFT, demonstrated less penalty. However, the PAM4 displayed the lowest performance. In contrast, the DQPSK with OIFFT performed similarly to the OOK also with the OIFFT. The DQPSK without the OIFFT demonstrated a degradation beyond 90 km. The DPSK with the OIFFT demonstrated the best result by far achieving 0.64 Tbps over 240 km. Albeit, the DPSK without the OIFFT had shown the worst degradation over 240 km. This difference can be explained by the extra crosstalk on adjacent carriers due to OIFFT absence mainly affected phase modulation formats. Thus, the AO-OFDM best results achieved 1.28 Tbps over 90 km of SSMF and 0.64 Tbps over 240 km of SSMF by DQPSK and DPSK respectively.

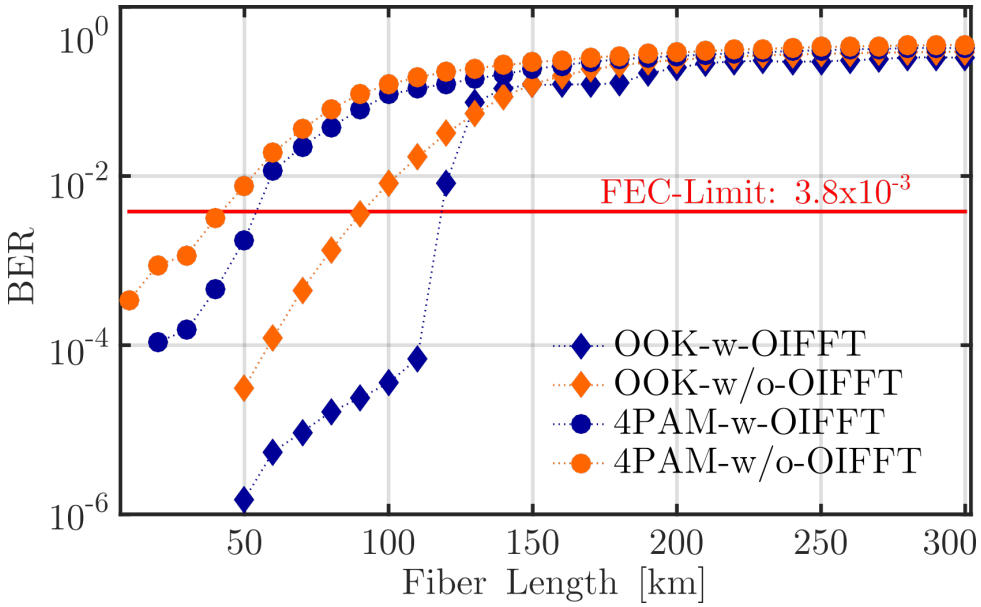

Figure 46 – OOK and PAM4 evaluation.

Furthermore, comparing the eye diagram of the 126th optical carrier in Fig. 47 also demonstrated the improvement caused by the OIFFT. The eye-opening for the OOK modulation after 60 km of SSMF is smaller, Fig. 47a, than the eye-opening for the OOK modulation after 110 km of SSMF, Fig. 47b, when the OIFFT was used. Similarly, in Fig. 47d, the DPSK eye-opening of the 126th optical carrier after 240 km of SSMF is more clear than the eye-opening, for the same carrier after 10 km of SSMF, Fig. 47c, when the OIFFT was not used. Thus, associating a modulation format such as DPSK naturally resistant to amplitude distortion, with a technique responsible to minimize crosstalk noise. Hence, it is not a surprise an increasing performance of the transmission system as here demonstrated.

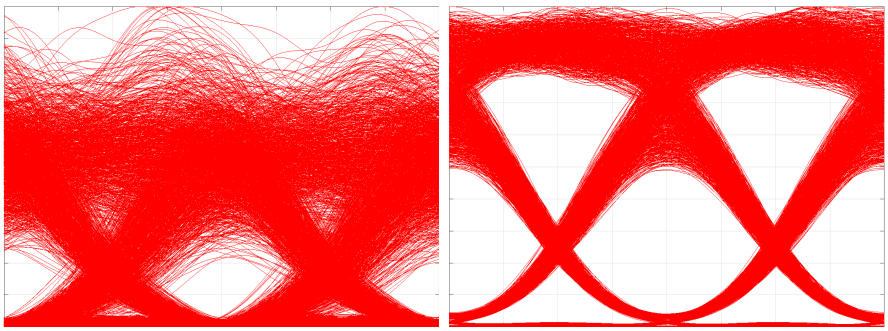

(a) OOK without the OIFFT. (b) OOK with the OIFFT.

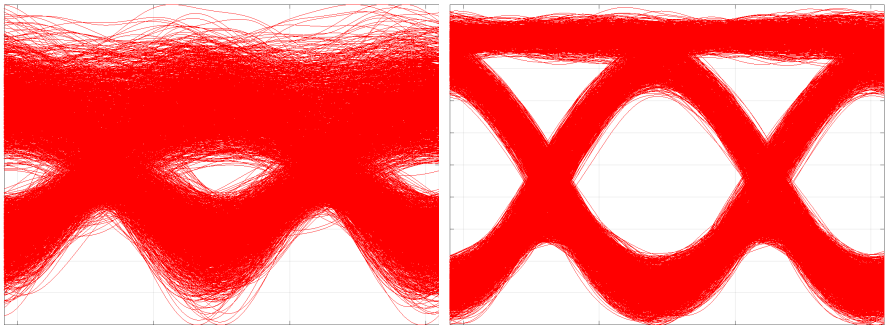

(c) DPSK without the OIFFT. (d) DPSK with the OIFFT.

Figure 47 – Comparing the eye diagrams between two different setups, one with the OIFFT and other without the OIFFT. a) A system without the OIFFT was transmitting an AO-OFDM signal over 60 km of SSMF with OOK modulation. b) A system with the OIFFT was transmitting an AO-OFDM signal over 110 km o SSMF with OOK modulation format. c) A system without the OIFFT was transmitting an AO-OFDM signal over 10 km of SSMF with DPSK modulation. d) A system with the OIFFT was transmitting an AO-OFDM signal over 240 km o SSMF with DPSK modulation format.

The ability to reduce cross talk interferences is the main characteristic of this setup which allows the OFDM signal to achieve further distances also it enables the possibility to add more carriers closer to each other hence increasing the whole system capability. Even more, as previously mentioned about the generation of multiple carriers from a single laser source, the carriers are orthogonally spaced from each other then just the set of MZI

could efficiently select one carrier apart from the others. On the other side, those newly created carriers will be closer to the noise floor hence less OSNR available for transmission. Thus, one future study can be evaluating the results of modulating each optical carrier with different modulation formats to better adapt to the available optical signal to noise rate (OSNR) on each optical carrier. As a result, the BER level per optical channel will decrease. The need for this work become clear when analysing Fig. 46 and 45 in another perspective.

For instance, observing the curve BER over a fiber length of each optical carrier shows the BER variation as shown in Fig. 48 for a DPSK modulation format. There, the first dimension (x) is an optical carrier, varying from 1 to 128 carrier, together with the second dimension (y), which is the fiber length varying from 10 to 300 km, compose the base of this three-dimensional graph. The third dimension (z) is the BER value ranging from zero displayed in blue, where no error is found, to red representing all values that are equal or greater than the FEC limit ($3.8x10^{-3}$).

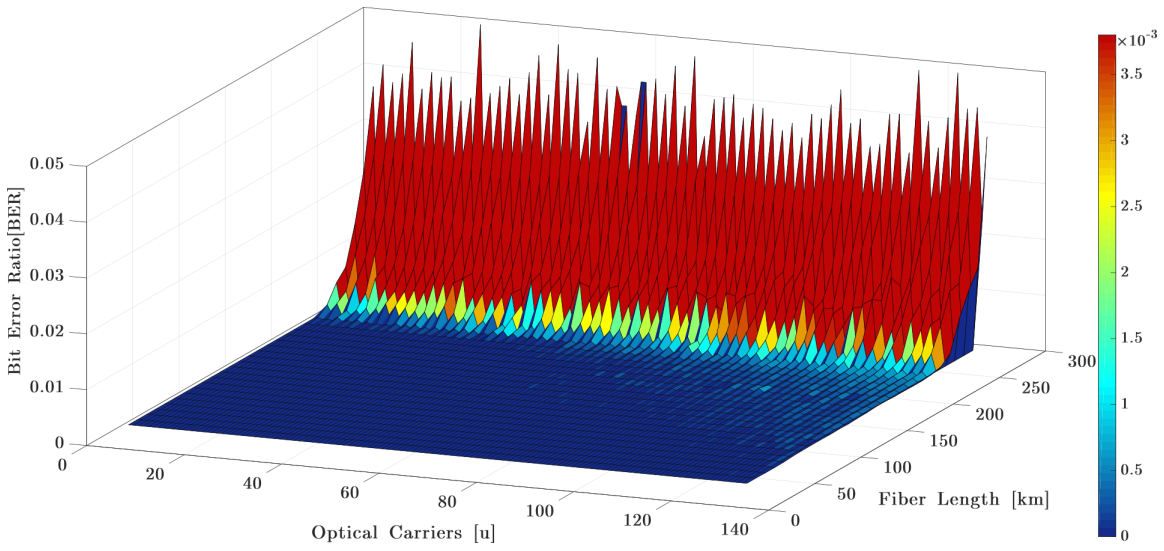

Figure 48 – BER over Optical Carrier over Fiber Length analysis for qualitative evaluation of how the OSNR varies among carrier due to the distance.

A top view from Fig. 48 is displayed in Fig. 49 allowing a better notion of how the BER varies from carrier to carrier across different lengths of glass fibre. There, two features are clearly shown, firstly half of all carriers do not show any error to any fibre lengths, and secondly the last optical carriers start to show bit errors sooner. The carriers in which significant bit error where not detected are the odd optical channels this can be explained by the fact that those light waves were recovered at the ONU side. Hence, they covered the exact distance shown on the graph, in contrast, the even carriers travel twice this distance additionally they not only approach the dispersion limit, eq. 1.1, of the glass fiber. Also, the last channels have less OSNR clearance than the first optical carriers as shown in Fig. 36.

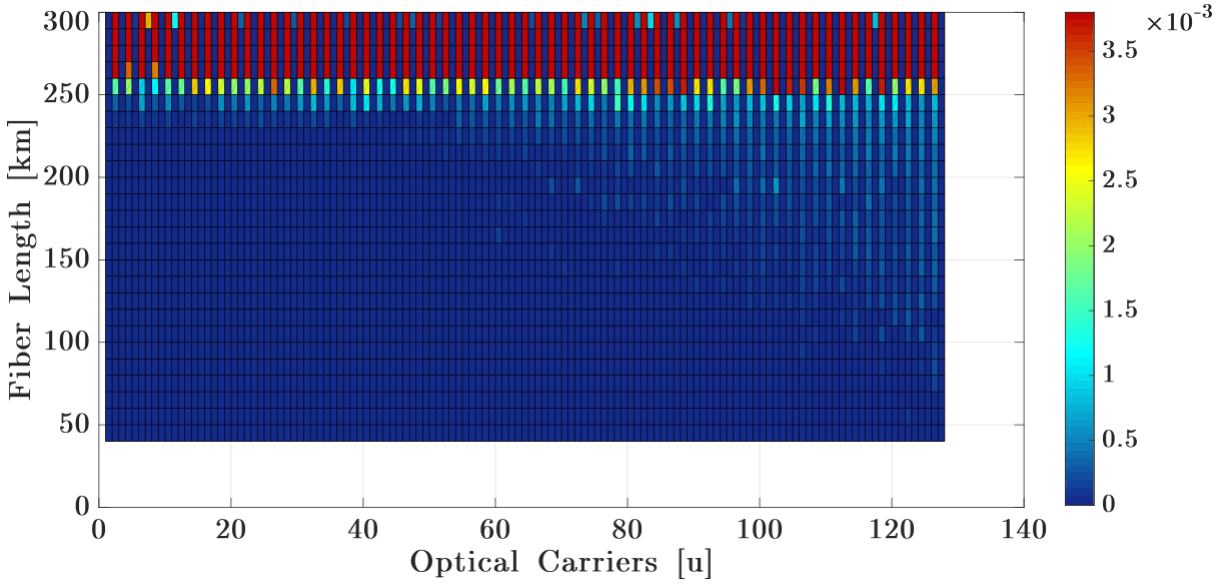

Figure 49 – DPSK top view of the BER over Optical Carrier over Fiber Length analysis.

Similar behaviour can be seen on a transmission using an OOK modulation as displayed in Fig. 50. Similarly, as a top view picture, the optical channels and the fiber length represent the base of the graph while the third dimension was characterised with a colour scale, ranging from blue to red meaning no error detected to over FEC limit error, respectively. At the OOK transmission covered a shorter distance as earlier mentioned. However, at transmission limit, odd channels show mostly any error until 110 km and last optical carriers also present bit errors earlier than carriers at the beginning of the AO-OFDM signal.

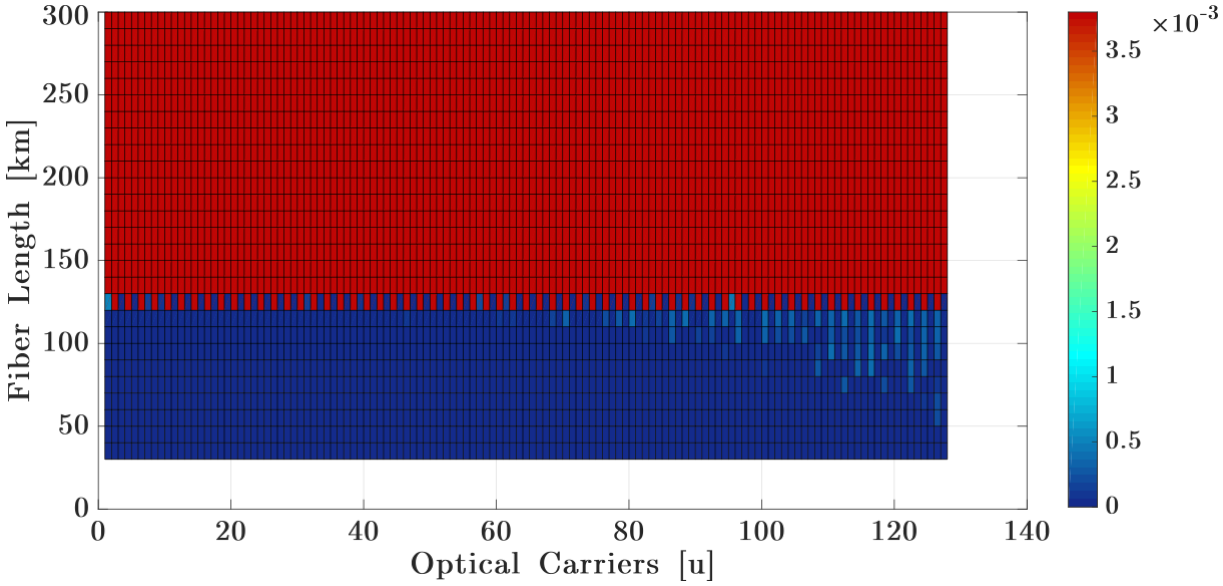

Figure 50 – OOK top view of the BER over Optical Carrier over Fiber Length analysis.

To better show the BER variation among optical channels a cut was extracted from Fig. 48 at the point with 250 km of SSMF and the DPSK modulation and this result is shown in Fig. 51. This graph shows each optical carrier by the BER value for its respective value, noticing that just the even carriers are here displayed as a result of no detecting errors at odd channels. Moreover, it is clear that, despite values fluctuations, an increasing trend is noticeable in which as the carrier index rises its respective bit error rate also increases. One possible explanation is the difference between each carrier of OSNR clearance, which decreases as the channel index grows.

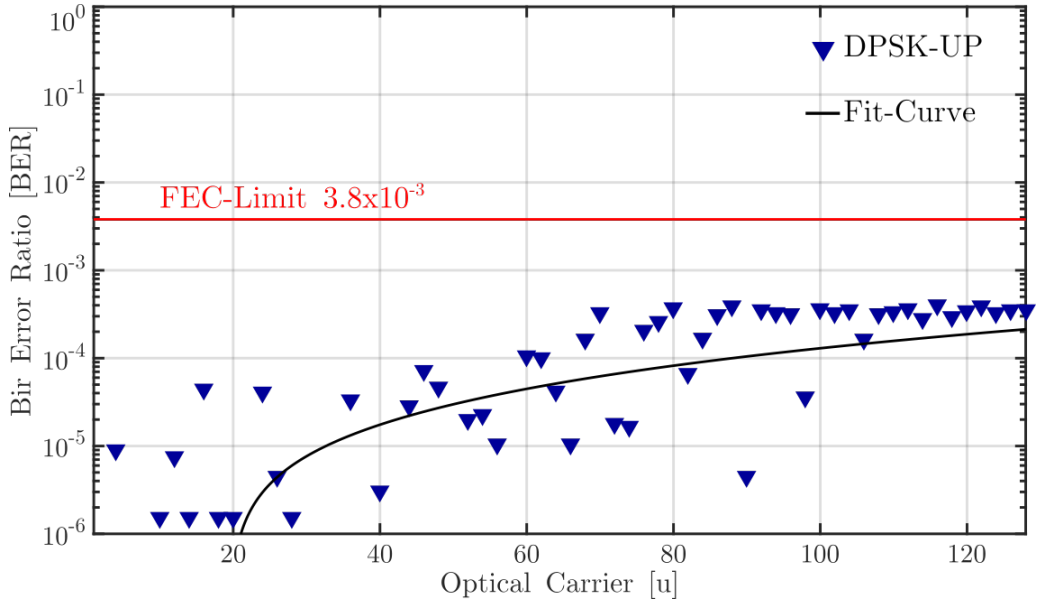

Figure 51 – DPSK front cut view at 250 km of SSMF of the BER over Optical Carrier over Fiber Length analysis one particular case of OSNR variation.

4.6 Papers produced

From this work, the main contribution was to achieve the implementation of AO-OFDM signal and apply it to transmit over 1.28bTps over 90 km of SSMF and 640 Gbps over 240 km of SSMF. Moreover, from this fact, two publications were presented in different conferences at national and international level besides the contribution here already mentioned for the laboratory where this research was conducted. The papers published are:

MARCIANO, P. et al. A new all-optical ofdm architecture for ng-pon2. In:v OPTICAL SOCIETY OF AMERICA. *Latin America Optics and Photonics Conference*. [S.l.], 2018. p. W3D–4.

COELHO, D. et al. New architecture proposal to enhance spectrum efficiency in multi-wavelength optical access networks. In: MOMAG - *Brazilian conference of Microwaves and Optical-eletronics*.

4.7 Conclusion and future works

This work presented the steps taken to validate the elements and the system built on our simulation, that was based on actual components tested on controlled experiments aimed to acquire its characteristics. Then, this work had shown the simulated modules responses, which will be fundamental for the whole simulation such as the OFC source, the different kinds of modulation formats and the system behaviour for multiple values of noise power. Thus, showing that our system has a very close behaviour as it is to be expected from actual devices. Albeit, some results did not approach to the theoretical response such as the PAM4 modulation format because of the heavy distortion on the signal amplitude caused by the set of MZI.

Furthermore, this work has shown one way to enhance the actual passive optical network (PON), that is predicted to attend an enormous demand with an exponentially growing trend. Hence, this work proposal was to make it possible for the network to achieve over 240 km of standard single mode fibre (SSMF) also deliver up to 1.2 Tbps within a single optical link. The method here shown was based on Mach-Zehnder Interferometers (MZIs) that were responsible for implementing the Fourier direct and inverse transforms on the optical domain. Thus, removing some significant complexities from the electronic section which may become a bottleneck for high data flow ratios once high-speed electronics are expensive and the analogue to digital converter (ADC) acquisition time is costly for the processing time. Hence, the receptor and transmitter optical complexity increase, however, the time to process an optical orthogonal frequency division multiplexing (OFDM) signal is instantaneously making possible higher speed communications processes.

This work also highlighted some drawbacks of using this setup such as the bandwidth available to transmit information. When analysing the impulsive response of each channel one may notice a sinc response with periodical repetition; hence optical channel pass-band roll-off narrowed the available bandwidth by 20%. Also, at this point the overlapping of the adjacent carriers is significant. It is due to the MZI setup construction because when the symbol period matches the period of the MZI transition infinite frequencies components are needed to compose the signal. When the symbol period is longer than the MZI switching time, the signal is stable and allow a more reliable response. Noticing the symbol period stretching means less bandwidth occupied by it, which is not a surprise as a conventional OFDM signal its symbols are also spread to add a cyclic prefix to avoid interferences. This work also increased each symbols time by adding a copy of itself at the end of the data hence mitigating partially the sinc response of the MZI setup. Moreover, those cascade MZIs were implemented as out-of-the-shelve devices, although future work can be done to make those devices integrated on a chip. Thus, reducing its footprint size as well as improving the whole setup response allowing a more flat response of the optical

channel's output.

Besides the MZI's response also the fact that higher modulation amplitude order is not suitable for this setup due the amplitude distortion, the all-optical fast Fourier transform implemented were here shown able to diminish cross talk noise among carriers significantly.

Thus, this work had shown that not only the all-optical OFDM signal would enhance the PON, aiming to enable the optical networks to attend this ever-growing demand. Also, this work shows the need for developing techniques to integrate those out-of-the-shelve components on a single chip and reduce total system cost and footprint size. Besides, future work can be developed on researching the discrete multi-tone applied for optical carriers as another approach to mitigating the MZIs impulsive response as well as the differences of OSNR among optical channels. Studies had shown higher order optical modulation with direct detection techniques concerning the next generation of passive optical networks [55, 56].

Bibliography

1 INDEX, C. V. N. The zettabyte era—trends and analysis, cisco. *Cisco company, June*, 2016. Cited 2 times in pages 8 and 17.

2 CISCO. *The zettabyte era: Trends and analysis*. 2015. Cisco Web Page. Cited on page. 17.

3 CISCO, W. P. Cisco visual networking index: Global mobile data traffic forecast update, 2016–2021. 2017. Cited on page. 17.

4 NESSET, D. Pon roadmap. *IEEE/OSA Journal of Optical Communications and Networking*, IEEE, v. 9, n. 1, p. A71–A76, 2017. Cited 3 times in pages 17, 18, and 21.

5 DHILLON, H. S.; HUANG, H.; VISWANATHAN, H. Wide-area wireless communication challenges for the internet of things. *IEEE Communications Magazine*, IEEE, v. 55, n. 2, p. 168–174, 2017. Cited on page. 18.

6 BINDHAIQ, S. et al. Recent development on time and wavelength-division multiplexed passive optical network (twdm-pon) for next-generation passive optical network stage 2 (ng-pon2). *Optical Switching and Networking*, Elsevier, v. 15, p. 53–66, 2015. Cited 2 times in pages 18 and 21.

7 KANI, J.-i. et al. Solutions for future mobile fronthaul and access-network convergence. *Journal of Lightwave Technology*, IEEE, v. 35, n. 3, p. 527–534, 2017. Cited on page. 18.

8 IEEE. *IEEE P802.3ca 100G-EPON Task Force*. 2018. Web Page. Cited on page. 18.

9 MILLER, S. E.; MARCATILI, E. A.; LI, T. Research toward optical-fiber transmission systems. *Proceedings of the IEEE*, IEEE, v. 61, n. 12, p. 1703–1704, 1973. Cited on page. 19.

10 SU, F. History and technology of wavelength division multiplexing. *SPIE Newsroom*, SPIE, n. 166, 1997. Acesso em: 24 June 2018. Cited on page. 19.

11 BACHUS, E.-J. et al. Ten-channel coherent optical fibre transmission. *Electronics letters*, IET, v. 22, n. 19, p. 1002–1003, 1986. Cited on page. 19.

12 KIM, K. S. On the evolution of pon-based ftth solutions. *Information sciences*, Elsevier, v. 149, n. 1-3, p. 21–30, 2003. Cited on page. 19.

13 DONG, P. et al. Four-channel 100-gb/s per channel discrete multitone modulation using silicon photonic integrated circuits. *Journal of Lightwave Technology*, IEEE, v. 34, n. 1, p. 79–84, 2016. Cited on page. 20.

14 EISELT, N. et al. First real-time 400g pam-4 demonstration for inter-data center transmission over 100 km of ssmf at 1550 nm. In: IEEE. *Optical Fiber Communications Conference and Exhibition (OFC), 2016*. [S.l.], 2016. p. 1–3. Cited on page. 20.

15 LI, X. et al. 4× 28 gb/s pam4 long-reach pon using low complexity nonlinear compensation. In: IEEE. *Optical Fiber Communications Conference and Exhibition (OFC), 2017*. [S.l.], 2017. p. 1–3. Cited on page. 20.

16 GUAN, P. et al. All-optical ultra-high-speed ofdm to nyquist-wdm conversion based on complete optical fourier transformation. *Journal of Lightwave Technology*, IEEE, v. 34, n. 2, p. 626–632, 2016. Cited on page. 20.

17 THORLABS. *Mach-40 086: Dual Parallel Modulator with RF detectors*. 2018. Web Page. Cited on page. 21.

18 AGRAWAL, G. P. Fiber-optic communication systems. In: _____. *Fiber-optic communication systems*. New Yourk: Wiley-Interscience, 2002. p. 37–55. Cited on page. 21.

19 ZEHNDER, L. *Ein neuer interferenzrefraktor*. [S.l.]: Springer, 1891. Cited on page. 23.

20 MACH, L. Ueber einen interferenzrefraktor. *Zeitschrift für Instrumentenkunde*, v. 12, n. 3, p. 89, 1892. Cited on page. 23.

21 REIDER, G. A. Photonics: An introduction. In: _____. *Photonics: An Introduction*. Vienna, Austria: Springer, 2018. p. 86–90. Cited on page. 24.

22 QU, K. et al. Ultra-flat and broadband optical frequency comb generator via a single mach–zehnder modulator. *IEEE Photonics Technology Letters*, IEEE, v. 29, n. 2, p. 255–258, 2017. Cited 2 times in pages 25 and 27.

23 IMRAN, M. et al. A survey of optical carrier generation techniques for terabit capacity elastic optical networks. *IEEE Communications Surveys & Tutorials*, IEEE, 2017. Cited on page. 28.

24 LIU, L. et al. A simplified tunable frequency interval optical frequency comb generator using a single continuous-wave laser. *Optoelectronics Letters*, Springer, v. 13, n. 2, p. 104–107, 2017. Cited on page. 28.

25 RAMASWAMI, R.; SIVARAJAN, K.; SASAKI, G. *Optical networks: a practical perspective*. [S.l.]: Morgan Kaufmann, 2009. Cited 2 times in pages 29 and 30.

26 KUNENE, G. *A History of Telecommunications: How Telecoms Became Just Another Interface*. 2018. Web Page. Cited on page. 30.

27 TANENBAUM, A. S.; WETHERALL, D. *Computer networks*. [S.l.]: Prentice hall, 1996. Cited on page. 31.

28 ARMSTRONG, J. Ofdm for optical communications. *Journal of lightwave technology*, IEEE, v. 27, n. 3, p. 189–204, 2009. Cited 4 times in pages 32, 34, 35, and 40.

29 STOTT, J. H. The how and why of cofdm. *EBU Technical review*, EUROPEAN BROADCASTING UNION, p. 43–50, 1998. Cited 3 times in pages 32, 35, and 40.

30 LASORTE, N.; BARNES, W. J.; REFAI, H. H. The history of orthogonal frequency division multiplexing. In: IEEE. *Global Telecommunications Conference, 2008. IEEE GLOBECOM 2008. IEEE*. [S.l.], 2008. p. 1–5. Cited on page. 33.

31 CHANG, R. W. Synthesis of band-limited orthogonal signals for multichannel data transmission. *Bell Labs Technical Journal*, Wiley Online Library, v. 45, n. 10, p. 1775–1796, 1966. Cited on page. 33.

32 LANGTON, C. *Orthogonal Frequency Division Multiplexing (OFDM) Tutorial*. 2013. Web page ComplexToReal. Cited on page. 35.

33 MARHIC, M. E. Discrete fourier transforms by single-mode star networks. *Optics letters*, Optical Society of America, v. 12, n. 1, p. 63–65, 1987. Cited on page. 37.

34 HILLERKUSS, D. et al. Simple all-optical fft scheme enabling tbit/s real-time signal processing. *Optics express*, Optical Society of America, v. 18, n. 9, p. 9324–9340, 2010. Cited 5 times in pages 37, 38, 45, 46, and 68.

35 LATHI, B. P. *Modern digital and analog communication systems*. [S.l.]: Oxford University Press, Inc., 2009. Cited 3 times in pages 38, 39, and 40.

36 WINZER, P. J.; ESSIAMBRE, R.-J. Advanced optical modulation formats. In: *Optical Fiber Telecommunications VB*. [S.l.]: Elsevier, 2008. p. 23–93. Cited 5 times in pages 40, 47, 49, 50, and 51.

37 ESSIAMBRE, R.-J. et al. Capacity limits of optical fiber networks. *Journal of Lightwave Technology*, IEEE, v. 28, n. 4, p. 662–701, 2010. Cited 3 times in pages 40, 41, and 42.

38 MATLAB. *AWG Channel*. 2018. Web Page. Cited on page. 41.

39 AGRAWAL, G. P. Fiber-optic communication systems. In: _____. *Fiber-optic communication systems*. New Yourk: Wiley-Interscience, 2002. p. 133–174. Cited on page. 42.

40 AGRAWAL, G. P. Fiber-optic communication systems. In: _____. *Fiber-optic communication systems*. New Yourk: Wiley-Interscience, 2002. p. 226–271. Cited on page. 42.

41 CHEN, X. et al. An osnr calculating method based on network topology for optical network. In: IEEE. *Optical Communications and Networks (ICOCN), 2017 16th International Conference on*. [S.l.], 2017. p. 1–3. Cited on page. 42.

42 YIN, G. et al. Reference optical spectrum based in-band osnr monitoring method for edfa amplified multispan optical fiber transmission system with cascaded filtering effect. *IEEE Photonics Journal*, IEEE, v. 10, n. 3, p. 1–10, 2018. Cited on page. 42.

43 AGRAWAL, G. P. Fiber-optic communication systems. In: _____. *Fiber-optic communication systems*. New Yourk: Wiley-Interscience, 2002. p. 183–219. Cited on page. 43.

44 AGRAWAL, G. P. Fiber-optic communication systems. In: _____. *Fiber-optic communication systems*. New Yourk: Wiley-Interscience, 2002. p. 158–169. Cited on page. 43.

45 FERREIRA, R. J. et al. All-optical fast fourier transform for processing an optical ofdm superchannel. In: IEEE. *Microwave and Optoelectronics Conference (IMOC), 2017 SBMO/IEEE MTT-S International*. [S.l.], 2017. p. 1–5. Cited on page. 44.

46 XU, J. et al. Optical interferometric synthesis of pam4 signals based on dual-drive mach–zehnder modulation. *Optics Communications*, Elsevier, v. 402, p. 73–79, 2017. Cited on page. 48.

47 KAMINOW, I.; LI, T.; WILLNER, A. E. *Optical fiber telecommunications VB: systems and networks*. [S.l.]: Elsevier, 2010. Cited 3 times in pages 49, 50, and 51.

48 SHEN, Y.; LU, K.; GU, W. Coherent and incoherent crosstalk in wdm optical networks. *Journal of lightwave technology*, IEEE, v. 17, n. 5, p. 759, 1999. Cited on page. 66.

49 TAKAHASHI, H.; ODA, K.; TOBA, H. Impact of crosstalk in an arrayed-waveguide multiplexer on n/spl times/n optical interconnection. *Journal of lightwave technology*, IEEE, v. 14, n. 6, p. 1097–1105, 1996. Cited on page. 66.

50 CHENG, N. et al. Reflective crosstalk cancellation in self-seeded wdm pon for mobile fronthaul/backhaul. *Journal of lightwave technology*, IEEE, v. 34, n. 8, p. 2056–2063, 2016. Cited on page. 66.

51 WEN, H. et al. First demonstration of six-mode pon achieving a record gain of 4 db in upstream transmission loss budget. *Journal of Lightwave Technology*, IEEE, v. 34, n. 8, p. 1990–1996, 2016. Cited on page. 66.

52 YU, Y.; TOWNSEND, P. D.; ZHAO, J. Equalization of dispersion-induced crosstalk in optical offset-qam ofdm systems. *IEEE Photonics Technology Letters*, IEEE, v. 28, n. 7, p. 782–785, 2016. Cited on page. 66.

53 TYCHOPOULOS, A.; KOUFOPAVLOU, O.; TOMKOS, I. Fec in optical communications-a tutorial overview on the evolution of architectures and the future prospects of outband and inband fec for optical communications. *IEEE Circuits and Devices Magazine*, IEEE, v. 22, n. 6, p. 79–86, 2006. Cited on page. 68.

54 KIM, H.; GNAUCK, A. H. Chirp characteristics of dual-drive. mach-zehnder modulator with a finite dc extinction ratio. *IEEE Photonics Technology Letters*, IEEE, v. 14, n. 3, p. 298–300, 2002. Cited on page. 70.

55 SEIMETZ, M.; NOELLE, M.; PATZAK, E. Optical systems with high-order dpsk and star qam modulation based on interferometric direct detection. *Journal of Lightwave Technology*, IEEE, v. 25, n. 6, p. 1515–1530, 2007. Cited on page. 83.

56 SOTIROPOULOS, N.; KOONEN, T.; WAARDT, H. de. Advanced differential modulation formats for optical access networks. *Journal of Lightwave Technology*, IEEE, v. 31, n. 17, p. 2829–2843, 2013. Cited on page. 83.